

# **INNOVATIONS IN FUZZY CONTROL AND BRAIN INSPIRED COMPUTATION**

*A Thesis*

*Submitted in partial fulfillment of the requirement for  
the Degree of  
Master of Electronics and Telecommunication Engineering*

Jadavpur University

May 2019

By

**Eashita Chowdhury**

Registration No: 137295 of 2016-2017

Examination Roll No:

M6IAR19005(001610704005)

*Under the Guidance of*

**Prof. Amit Konar**

Department of Electronics and Telecommunication Engineering

Jadavpur University, Kolkata-700032

India

FACULTY OF ENGINEERING AND TECHNOLOGY

JADAVPUR UNIVERSITY

## **CERTIFICATE**

This is to certify that that the dissertation entitled “**Innovations in fuzzy control and Brain Inspired Computation**” has been carried out Eashita Chowdhury (University Registration No: 137295 of 2016-2017) under my guidance and supervision and be accepted in partial fulfillment of the requirement for the Degree of Master of Electronics & Telecommunication Engineering. The research results presented in the thesis have not been included in any other paper submitted for the award of any degree to any other University or Institute.

---

Prof. Amit Konar(Supervisor)

Dept. of Electronics & Telecommunication Engineering

Jadavpur University

---

Prof. Sheli Sinha Chaudhuri

Head of the Department

Electronics & Telecommunication Engineering

Jadavpur University

---

Prof. Chiranjib Bhattacharjee

Dean, Faculty Council of Engineering and Technology

Jadavpur University

FACULTY OF ENGINEERING AND TECHNOLOGY  
JADAVPUR UNIVERSITY

**CERTIFICATE OF APPROVAL\***

The forgoing thesis is hereby approved as a creditable study of an engineering subject and presented in a manner satisfactory to warrant acceptance as prerequisite to the degree for which it has been submitted. It is understood that by this approval the undersigned do not necessarily endorse or approve any statement made, opinion expressed or conclusion drawn there in but approve the thesis only for which it is submitted.

**Committee on final examination**

**For the evaluation of the thesis**

---

Signature of the Examiner

\*Only in the case the thesis is approved

FACULTY OF ENGINEERING AND TECHNOLOGY  
JADAVPUR UNIVERSITY

**DECLARATION OF ORIGINALITY AND COMPLIANCE OF  
ACADEMIC THESIS**

I hereby declare that the thesis entitled “**Innovations in fuzzy control and Brain Inspired Computation**” contains literature survey and original research work by the undersigned candidate, as part of his Degree of Master Technology in Intelligent Automation and Robotics .

All information have been obtained and presented with academic rules and ethical conduct.

I also declare that, as required by these rules and conduct, I have fully cited and referenced all materials and results that are not original to this work.

**Name:** EASHITA CHOWDHURY

**Class Roll No:** M6IAR19005(001610704005)

**Thesis Title:** **Innovations in fuzzy control and Brain Inspired Computation**

---

Signature of the candidate

## **ACKNOWLEDGEMENT**

First and foremost, I would like to express my earnest gratitude and heartfelt indebtedness to my supervisor, Prof. Amit Konar, Department of Electronics and Tele - communication Engineering, for the privilege and the pleasure, of allowing me to work under him towards my Degree of Master of Electronics & Telecommunication Engineering. This work would not have been materialized, but for his whole-hearted help and support. Working under him has been a great experience. I sincerely thank my supervisor, particularly for all the faith he had in me.

I am thankful to Prof. Sheli Sinha Chowdhury who has acted as Head of the Department of Electronics and Telecommunication Engineering during the tenure of my studentship. I would also like to show my special gratitude to Miss. Lidia Ghosh and Mrs Mousumi Laha, PhD Research Scholar of the Department of Electronics and Telecommunication Engineering and Mr Zeeshan Qadir , my classmate for her constant guidance and valuable advices.

I am indebted to my classmates and friends for their constant support and good wishes. Lastly, I would like to thank my parents and sister for their love, support and guidance through the course work.

Date

Place: Jadavpur University

Eashita Chowdhury

Class Roll No.:001610704005

## **PREFACE**

The logic of fuzzy sets has proved its excellence in real world applications of diverse domains. The thesis makes an humble attempt to develop new and upcoming applications of fuzzy logic in next generation engineering systems. Four typical applications of fuzzy logic in real world systems are proposed. The first application deals with control of pH by fuzzy decision making. The second application is concerned with EEG-based classification of fingers from finger tapping experiments. The third application refers to the analysis of functional near Infrared Spectroscopic images to classify individual finger movements. The last topic includes an analysis of cognitive load of the subject in a virtual-reality environment. Each topic is discussed with sufficient details, narrating the problem-description, approach, analysis, experiments and main results obtained at the end of the experiment.

The thesis includes 7 chapters. Chapter 1 provides an introduction to the logic of fuzzy sets. It is primarily a review of existing works on fuzzy sets, but carries a mission to develop challenging applications of the proposed concepts of fuzzy sets in the subsequent chapters of the thesis. Chapter 2 provides a foundation to Brain-Computer Interfaces. It deals with brain signals and the basic steps required to detect the signature of the acquired brain signals. Chapter 3 includes the control of pH of mixture of acids and bases by neuro fuzzy PID controller. Chapter 4 is an original contribution of the thesis. It demonstrates the scope of brain- computer interface to detect individual fingers from their motor imageries. Chapter 5 outlines the sequence of steps involved to detect fingers from their motor imageries by employing functional

Near Infrared Spectroscopy devices. Chapter 6 examines a very recent problem of great interest to the community of cognitive science. It deals with the analysis of the cognitive load of the subject in a virtual reality(driving) environment using encephalographic means. Concluding remarks are appended at the end of the thesis in Chapter 7.

# Contents

## Chapter 1:

### Introduction to Fuzzy

1.1	Introduction	1.2
1.2	Membership functions	1.3
1.3	Operation on Fuzzy Sets	1.7
1.4	Fuzzy Max- Min and Max- Product Composition	1.8
1.5	Type I Fuzzy Sets	1.9
1.6	Type II Fuzzy sets	1.12
1.7	Scope of theThesis	1.12
	<i>References</i>	1.13

## Chapter 2:

### Introduction to Brain Computer Interface

2.1	Introduction	2.2
2.2	History	2.4
2.3	Steps Involved in BCI	2.5
2.4	Signal Acquisition Method	2.8
2.5	Non Invasive Recording Methods	2.9
2.6	Invasive Recording Methods	2.19



2.7	Brain Signal Patterns for BCI operation	2.21
	<i>References</i>	2.27

*Chapter 3:*  
*Fuzzy chemistry and fuzzy based pH Controller*

3.1	Introduction	3.2
3.2	Fuzzy chemistry	3.3
3.3	Membership function in fuzzy chemistry	3.5
3.4	Fuzzy pH controller	3.7
3.5	Conclusion a	3.10
	<i>References</i>	3.12

*Chapter 4:*  
*EEG Based finger induced Motor Imageries by Type-II Fuzzy*

4.1	Introduction	4.2
4.2	System Overview	4.3
4.3	Classifier Design	4.4
4.4	Experiments and Results	4.5

4.5	Classifier Performance and Statistical Validation	4.9
4.6	Conclusion	4.12
	<i>References</i>	4.13

*Chapter 5:*  
*Finger induced Motor Imageries from Hemodynamic response using Type-II Fuzzy*

5.1	Introduction	5.2
5.2	Principles and Methodology	5.5
5.3	Classifier Design	5.7
5.4	Experiments and Results	5.7
5.5	Classifier Performance and Statistical Validation	5.12
5.6	Conclusion	5.15
	<i>References</i>	5.16

Chapter 6:  
VR Based Cognitive Load Test

6.1	Introduction	6.1
6.2	Methodology	6.3
6.3	Classifier Design	6.6
6.4	Experiments and Results	6.9
6.5	Conclusion	6.11
	<i>References</i>	6.13

Chapter 7:  
Conclusion

7.1	Self Review of theThesis	7.1
-----	--------------------------	-----

## List of Figures

Fig. 1.1	The membership curve for the $\gamma$ function	1.4
Fig. 1.2	The membership curve for the $s$ function	1.4
Fig. 1.3	The membership curve for the $L$ function	1.5
Fig. 1.4	Triangular membership function	1.6
Fig. 1.5	The membership curve for the $\pi$ function	1.6
Fig. 1.6	The membership curve for the Gaussian function	1.7
Fig. 1.7	Type I Fuzzy Sets	1.9
Fig. 1.8	Foot of Uncertainty of IT2FS	1.10
Fig. 1.9	Interval Type II Fuzzy sets	1.11
Fig. 1.10	Gaussian Type 2 Fuzzy sets	1.12
Fig2.1	Overview of a general BCI system framework	2.8
Fig2.2	Classification of BCI system	2.9
Fig2.3	Comparison of different signal acquisition methods	2.10

Fig 2.4	The 10/20 international system of electrode placement	2.14
Fig 2.5	BCI research article	2.14
Fig 2.6	Brain signal patterns for BCI operation	2.23
Fig3.1	Fuzzy membership for chemical properties	3.3
Fig3.1	Fuzzy controller	3.5
Fig4.1	Block diagram of the system	4.3
Fig4.2	Architecture of the Type 2 Fuzzy classifier	4.5
Fig4.3	Stimuli representation of individual fingers	4.6
Fig4.4	3D view of the activation regions of individual fingers	4.6
Fig4.5	Brain activation regions of individual fingers	4.7
Fig4.6	After filtering and artifact removal of individual fingers	4.8
Fig4.7	PSD extraction of the fingers from motor cortex and pre frontal region	4.9
Fig5.1	System overview of finger classification	5.6
Fig5.2	Experimental set up and source detector connection of motor cortex	5.8
Fig5.3	Sample signal trial of visual cue for finger induced motor imagery	5.10
Fig5.4	Feature level discrimination between mean concentration of five fingers	5.11
Fig5.5	Brain activation regions of individual fingers	5.12
Fig6.1	Construction of flat top IT2FS	6.6
Fig6.2	Secondary membership assignment	6.6
Fig6.3	Firing strength computation in the proposed GT2FS classifier	6.7

## List of Tables

Table 2.1	Summary of the brain data acquisition methods	2.6
Table 2.2	Different categories of brainwave patterns	2.12
Table 4.1	Classification accuracy of five fingers	4.10
Table4.2	Confusion matrix for classes	4.10
Table4.3	Relative performance analysis of individual fingers	4.11
Table4.4	Statistical analysis with the reference	4.12
Table5.1	Comparison between PCA and proposed feature selection with IT2FS	5.12
Table5.2	Relative performance analysis of individual fingers	5.13
Table5.3	Statistical analysis with the reference	5.14
Table 5.4	Comparison between classification accuracy of proposed and existing method	5.15
Table 5.4	Comparison between classification accuracy of proposed and existing method	5.15
Table 6.1	Classification accuracy without and with VR	6.9
Table 6.2	Statistical analysis with the reference algorithm	6.10

# 1

## Introduction to Fuzzy Logic

**Abstract-** A fuzzy Logic is an extended form of Boolean Logic proposed by Lotfi Zadeh in 1965 which is based on mathematical theory of fuzzy is a generalization of the classical propositional and predicate logic. In real world we usually deal with some sort of uncertainty. Fuzziness is the uncertainty that arises from linguistic concepts without clear borders. Generally fuzzy logic provides flexibility for reasoning which enables to state true or false or gives digital value 0 or 1. In natural language, many statements are vague, or fuzzy. For example, classifying a certain objects 'large' leaves us with an uncertainty of how large this object really is. Fuzzy concepts is always modeled by a degree of membership  $\mu$ . Fuzziness in software applications is useful for making user interactions more natural. For example, fuzziness in databases can lead to more intuitive and simpler queries.

## 1.1 Introduction

There is always a uncertainty to build a fuzzy system. This means that the output should be no longer a crisp number since uncertainty has been propagated to the output as a result of uncertain information and inputs. Therefore the output should somehow represent this uncertainty. This is the reason why ordinary fuzzy logic systems called Type 1 Fuzzy Logic Systems that gives away to Type-II fuzzy logic systems (T2FLSs)[1,4]. The idea of T2FS proposed by Zadeh is an answer to the uncertainties because it features a fuzzy membership triggered by so called fuzzy set. The viability of T2FS is in practice hindered by its demanding computational cost, attributed by the type reduction procedure from Type-2 to Type-1. Therefore this noise has led to an interval Type- 2 Fuzzy System(IT2FS)[2], which presents a simplified version of the pure T2FS. The IT2FS is a special case of T2FS which assumes a secondary grade of the type 2 membership functions to be unity to mitigate the computational burden. Evolving Fuzzy System is a research area of growing interest for learning from data streams. Even so most EFS are generally built upon the T1FS which possesses a crisp and certain membership. The T1FS is not robust with uncertainties in the data representation which can be viewed in the inexact, inaccurate and uncertain characteristics of real world data streams.

The four main sources of uncertainty as follows :

- The linguistic words which are used in both antecedent and consequents of the fuzzy rules means differs from person to person
- There are some consequents derived from the insights of different experts, may vary for person.



- The interference of noise have applications in the real world.
- The measuring devices which provide the inputs to fuzzy systems introduces noise to the inputs.

## 1.2 Membership Functions:

The grade of membership<sup>[3]</sup>  $\mu_A(x)$  maps the object or its attribute  $x$  to positive real numbers in the interval  $[0, 1]$ . Because of its mapping characteristics like a function, it is called membership function.

Definition 2.2: A membership function  $\mu_A(x)$  is characterized by the following mapping:

$$\mu_A: x \rightarrow [0,1], x \in X$$

where  $x$  represents the real number describing an object or its attribute and  $X$  is the universe of discourse and  $A$  is a subset of  $X$ .

**Typical Membership Functions:** There are four typical membership functions namely triangular, Gaussian (bell-shaped), S-function and  $\gamma$ -Function are commonly used.

### 1.2.1 The $\gamma$ -Function

There are two parameters  $\alpha$  and  $\beta$

$$\begin{aligned} \gamma(\mu; \alpha, \beta) &= 0, & \mu &\leq \alpha \\ &= (\mu - \alpha) / (\beta - \alpha) & \alpha < \mu &\leq \beta \\ &= 1 & \mu &> \beta \end{aligned}$$

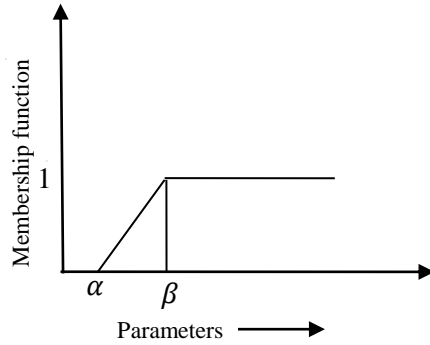


Fig 1.1 The membership curve for the  $\gamma$  function

### 1.2.2 The s-function

This is mainly defined by its lower limit  $\alpha$ , its upper limit  $\gamma$ , and the value  $\beta$  which is the point of inflection  $\beta = (\alpha + \gamma)/2$  is the most application in fuzzy logic

so that  $\alpha < \beta < \gamma$

It is defined as

$$\begin{aligned}
 S(\mu; \alpha, \beta, \gamma) &= 0, & \mu &\leq \alpha \\
 &= 2[(\mu - \alpha)/(\gamma - \alpha)]^2, & \alpha < \mu &\leq \beta \\
 &= 1 - 2[(\mu - \gamma)/(\gamma - \alpha)]^2 & \beta < \mu &\leq \gamma \\
 &= 1 & \mu &> \gamma
 \end{aligned}$$

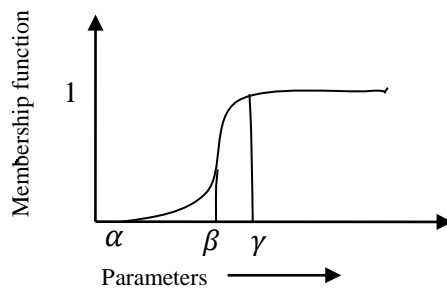


Fig 1.2 Membership curve for s-function

### 1.2.3 The L-function

This is a converse of  $\gamma$  function. It can be expressed as

$$\begin{aligned}
 L(\mu; \alpha, \beta) &= 1, & \mu < \alpha \\
 &= (\alpha - \mu) / (\beta - \alpha), & \alpha < \mu \leq \beta \\
 &= 0 & \mu > \beta
 \end{aligned}$$

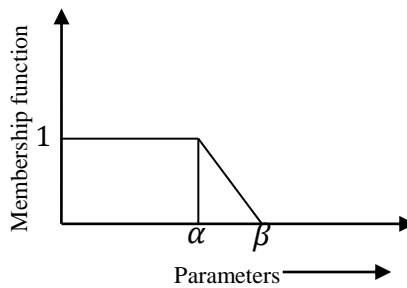


Fig 1.3 Membership curve of L-function

### 1.2.4 The Triangular membership function

This is also defined by the straight lines which is triangle in shape.

$$\begin{aligned}
 \Delta(\mu; \alpha, \beta, \gamma) &= 0, & \mu \leq \alpha \\
 &= (\mu - \alpha) / (\beta - \alpha), & \alpha < \mu \leq \beta \\
 &= (\alpha - \mu) / (\beta - \alpha) & \beta < \mu \leq \gamma \\
 &= 0 & \mu > \gamma
 \end{aligned}$$

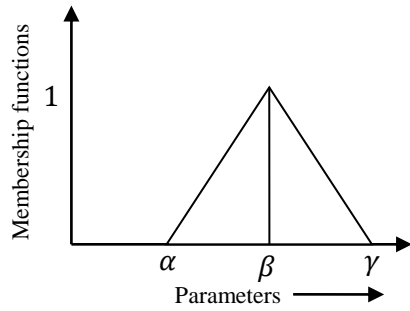


Fig 1.4 Triangular membership function

### 1.2.5 The $\pi$ function

It is better representation of fuzzy linguistic variables.

$$\begin{aligned} \pi(\mu; \alpha, \beta, \gamma, \delta) &= 0, & \mu &\leq \alpha \\ &= (\mu - \alpha) / (\beta - \alpha), & \alpha < \mu &\leq \beta \\ &= 1, & \beta < \mu &\leq \gamma \\ &= (\gamma - \mu) / (\delta - \gamma) & \gamma < \mu &\leq \delta \\ &= 0 & \mu &> \delta \end{aligned}$$

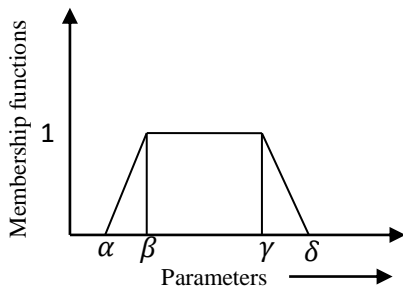


Fig 1.5 Membership curve of  $\pi$  function

### 1.2.6 The Gaussian membership Function

This function links between fuzzy systems and radial basis function (RBF) neural networks. It is represented by

$$G(\mu; c, x) = \exp[-\{(\mu-c)/\sqrt{2x^2}\}]$$

Here  $c$  is the centre and  $x$  is the width of membership function

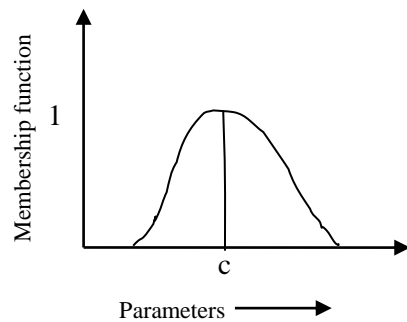


Fig 1.6 Membership curve of Gaussian function

### 1.3 Operation on Fuzzy sets:

There are mainly three types of operations on fuzzy sets namely as described below:

#### 1.3.1 Fuzzy T-Norm

The intersection of fuzzy set is defined by a T-norm[3] operator of two fuzzy sets A and B with a same universe of discourse X

$$\mu_{A \cap B}(X) = T(\mu_A(X), \mu_B(X))$$

T norm for the following conditions for membership values  $a$ ,  $b$ ,  $c$  and  $d$  and a function  $T : [0,1] \times [0,1] \rightarrow [0,1]$  satisfies the below characteristics is known as T-norm.

Commutativity:  $T(a,b) = T(b,a)$

Boundary:  $T(0,0) = 0$ ,  $T(a,1) = T(1,a) = a$

Monotonicity:  $T(a,b) \leq T(c,d)$  if  $a \leq c$ ,  $b \leq d$

Associativity:  $T(a, T(b, c)) = T(T(a, b), c)$

### 1.3.2 Fuzzy S-Norm

The union of fuzzy set is defined by a S-norm [3] for two fuzzy sets A and B under the same universe of discourse X.

$$\mu_{A \cup B}(X) = S(\mu_A(X), \mu_B(X))$$

S norm for the following conditions for membership values a, b, c and d and a function  $S: [0, 1] \times [0, 1] \rightarrow [0, 1]$  satisfies the below characteristics is known as T-norm.

Commutativity:  $S(a, b) = S(b, a)$

Boundary:  $S(0, 0) = 0$ ,  $S(a, 1) = S(1, a) = a$

Monotonicity:  $S(a, b) \leq S(c, d)$  if  $a \leq c$ ,  $b \leq d$

Associativity:  $S(a, S(b, c)) = S(S(a, b), c)$

### 1.3.3 Fuzzy Complement

The fuzzy complement[3] of fuzzy set A maps the transformation of membership function of A into the membership function of complement of A which is represented by  $A^c$  under the common universe of discourse X. Any function  $c: [0, 1] \rightarrow [0, 1]$  satisfies the below mentioned conditions

$$c[\mu_A(X)] = \mu_{A^c}(X)$$

Boundary:  $c(0) = 1$ ,  $c(1) = 0$

Non increasing condition: if  $a < b$  then  $c(a) \geq c(b)$  (a and b are two fuzzy membership)

## 1.4 Fuzzy Max-Min and Max-Product Composition Operation

The max-min composition[3] of two fuzzy relations A and B which is defined on  $X \square Y$  and  $Y \square Z$

$$C = A \circ B$$

$$\{ \mu_C(a, c) / (a, c) \}$$

where  $\mu_C(a, c) = \max\{\min(\mu_A(a, b), \mu_B(b, c)) / a \in A, b \in B, c \in C\}$

## 1.5 Type I Fuzzy sets

Type 1 fuzzy set has been proposed by Zadeh . This has many application such as time series production. A type-1 fuzzy set[4] is a set in which the membership function maps to the real unit interval  $[0,1]$ . For a crisp set the membership function is either 0 or 1.

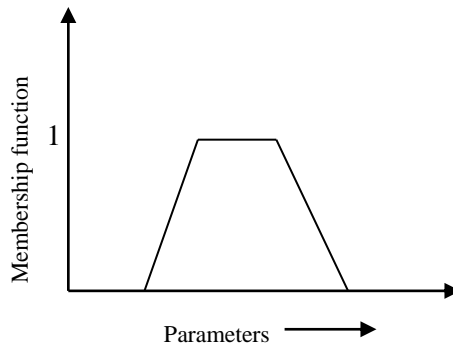


Fig 1.7 Type I Fuzzy Sets

## 1.6 Type II Fuzzy sets

This unifies the uncertainty where the membership function maps to the fuzzy subset of  $[0,1]$ . It is defined as follows:

**Definition 1** : A Type-II fuzzy set[1], denoted by  $\tilde{A}$ , is characterized by  $\mu_{\tilde{A}}(x, c)$  where  $x \in X$  and  $c \in J_x \subseteq [0, 1]$ .

$$\tilde{A} = \{ (x, c), \mu_{\tilde{A}}(x, c) / \forall x \in X, \forall c \in J_x \subseteq [0, 1] \} \text{ where } 0 \leq \mu_{\tilde{A}}(x, c) \leq 1$$

$$\tilde{A} = \iint \mu_{\tilde{A}}(x, c) / (x, c) J_x \subseteq [0, 1], x \in X \text{ and } c \in J_x$$

where the integral sign represents the union over all admissible  $x, c$ .  $\int$  is replaced by the  $\Sigma$  in the discrete T2FS.

**Definition 2:** The secondary membership has the domain known as primary membership and represented by  $J_x$ .

**Definition 3:** The secondary grade is determined by the amplitude of a secondary membership. The representation of secondary grade at  $x = x', c = c'$  is  $\mu_{\tilde{A}}(x = x', c = c')$ .

**Definition 4:** The bounded region is created by the union of the primary membership grades known as footprint of uncertainty (FOU)[5], i.e.,  $FOU \tilde{A} = \coprod_{x \in X} J_x$ .

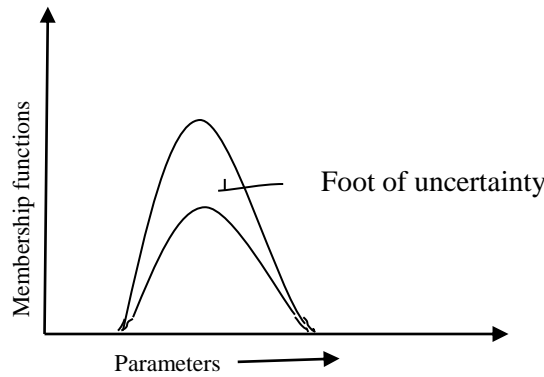


Fig 1.8 Foot of uncertainty of IT2FS

**Definition 5:**  $\tilde{A}$  is an embedded Type-II set of a general T2FS whereas  $\tilde{A}_e$  is a T2FS such that for every admissible  $x \in X$  in  $\tilde{A}_e$  there is one element, say  $c_x$ , in domain of  $\tilde{A}_e(x)$ , such that

$$\tilde{A}_e(x, c_x) = \tilde{A}(x, c_x), \text{ For a discrete T2FS}$$

$$\tilde{A} = \sum_{a=1}^K \sum_{b=1}^L \mu_{\tilde{A}}(x_a, c_{ab}) / (x_a, c_{ab}), J_{x_c} \subseteq [0, 1].$$



**Definition 6 :** A Type 1 embedded FS is same as to Type 2 embedded one except that the secondary grade is not there so the result is in the form of a Type-I fuzzy set. For a general T2FS,  $\tilde{A}$  is written as  $A_e$  which can be given by

$$A_e = \sum_{a=1}^K c_a / x_a, c_a \in J_{x_c}$$

**Definition 7 :** The upper and lower limits of FOU are Upper membership function and a Lower MF are two Type-I Membership Functions .

### 1.6.1 Interval Type 2 fuzzy set

An interval Type-II fuzzy set (IT2FS) is general T2FSs for which the grade of secondary membership is 1. In IT2FS [2,6] the main thing which is responsible is footprint of uncertainty(FOU). When the secondary membership functions belongs to the domain of a T2FS are interval Type-I membership functions, then it is called interval Type-II fuzzy set (IT2FS).

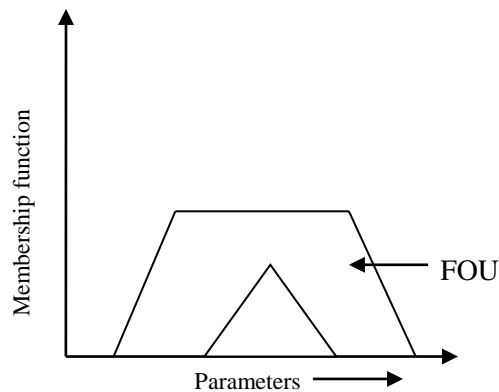


Fig 1.9 Interval Type II Fuzzy

### 1.6.2 Gaussian Type 2 fuzzy set

In this fuzzy set the secondary membership function belongs to the domain of T2FS are Type 1 Gaussian Membership functions is known as Gaussian Type 2 fuzzy set[7] The grade of membership function belongs to [0,1]

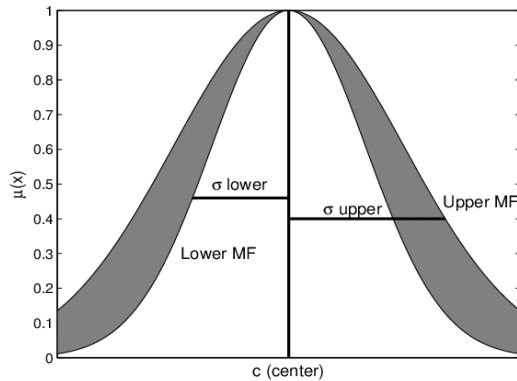


Fig 1.10 Gaussian Type-2 Fuzzy

## 1.7 Scope of the Thesis

It mainly deals with the approach of fuzzy in all the mentioned objectives discussed in the following chapters with the aim to fulfill it. Firstly in the dynamic approach for the mixture of acid and bases pH control by fuzzy decision making . Secondly finger induced motor imagery by EEG and the classifier is interval type II fuzzy set. Thirdly finger induced motor imagery classification by fNIRS and the fuzzy approach has been introduced there .Fourthly Cognitive load test while driving in a virtual Reality environment by EEG using a fuzzy classifier.

## **References**

1. □ Karnik, N. N., & Mendel, J. M.). Introduction to type-2 fuzzy logic systems. In 1998 IEEE International Conference on Fuzzy Systems Proceedings. IEEE World Congress on Computational Intelligence (Cat. No. 98CH36228) (Vol. 2, pp. 915-920). IEEE (May, 1998)
2. □ Liang, Q., & Mendel, J. M. Interval type-2 fuzzy logic systems: theory and design. IEEE Transactions on Fuzzy systems, 8(5), 535-550. (2000).
3. □ Konar, A. Computational intelligence: principles, techniques and applications. Springer Science & Business Media. (2006).
4. □ John, R., & Coupland, S. (2006). Extensions to type-1 fuzzy logic: Type-2 fuzzy logic and uncertainty. Computational Intelligence: Principles and Practice, 89-101.
5. □ Sepulveda, R., Melin, P., Díaz, A. R., Mancilla, A., & Montiel, O.. Analyzing the effects of the footprint of uncertainty in type-2 fuzzy logic controllers. Engineering Letters, 13(2), 138-147. (2006)
6. □ Castillo, O., Amador-Angulo, L., Castro, J. R., & Garcia-Valdez, M. A comparative study of type-1 fuzzy logic systems, interval type-2 fuzzy logic system and generalized type-2 fuzzy logic systems in control problems.. Information Sciences 354, 257-274(2016).
7. □ Karnik, N. N., & Mendel, J. M.. Centroid of a type-2 fuzzy set. Information Sciences, 132(1-4), 195-220. (2001)

# 2

## Introduction to Brain Computer Interface

**Abstract-** Many laboratories have begun to explore brain–computer interface (BCI) technology as a radically new communication option for those with neuromuscular impairments that prevent them from using conventional augmentative communication methods over the past decade. BCIs provide these users with communication channels that do not depend on peripheral nerves and muscles. They have the potential to offer humans a new and innovative non muscular modality through which one can communicate directly via their brain activity with their environment. These systems rely on the acquisition and interpretation of the commands encoded in neuro physiological signals without using the conventional muscular output pathways of the central nervous system (CNS). Apart from this, it has become, over the decades, one of most reliable tool for the scientific and detailed understanding of human psychology. Through this chapter we try to provide a detailed introduction to BCI, in terms of the major steps involved in BCI, its signal acquisition methods, how its signal quality could be improved and lastly some important feature selection and classification techniques.

## 2.1 Introduction

Human-computer interaction has been a topical research concept since the birth of the computer era. Methods of computer interaction have progressed rapidly over the years from cards with punched holes to keyboards and mice. Today there exist a multitude of innovative technologies that allow humans to interface with computers for the purposes of data entry, control or communication. Most of the efforts over the years have been dedicated to the design of user-friendly and ergonomic systems to produce a more efficient and comfortable means of communication. Interfaces such as voice recognition, gesture recognition and other technologies based on physical movement have received enormous research attention over the years and successful examples of these technologies are being rolled out commercially as a consequence.

The past two decades have seen an explosion of scientific interest in a completely different and novel approach of interacting with a computer. Inspired by the social recognition of people who suffer from severe neuromuscular disabilities, an interdisciplinary field of research has been created to offer direct human computer interaction via signals generated by the brain itself. Brain-Computer Interface (BCI) technology, as it is known, is a revolutionary communication channel that enables users to control computer applications through thoughts alone. It is defined as ‘A brain-computer interface is a communication system that does not depend on the brain’s normal output pathways of peripheral nerves and muscles’ [1]. The development of the cognitive neuroscience field has been instigated by recent advances in brain imaging technologies such as Electroencephalography (EEG), Magnetoencephalography (MEG)

and functional magnetic resonance imaging (fMRI). EEG is an imperfect and distorted indicator of brain activity, yet the fact that it can be acquired cheaply, is non-invasive and demonstrates direct functional correlations with high temporal resolution makes it the only practical direct brain computer communication channel. It is a new and challenging medium for us to exploit in a similar manner to the other communication modalities such as voice or vision. The endless potential of tapping into human brain signals may see the fantasies of science fiction writers becoming reality in the future.

The growing field of BCI research is however in its infancy. First signs of BCI research can be dated back to the early 1970s. The work of Dr. J. Vidal and his military research group at UCLA is cited as the first successful BCI implementation endeavor [2]. The current goal of BCI research is to develop replacement communication and control means for severely disabled people. For those who have lost all voluntary muscle control, referred to as locked-in syndrome, BCI technology offers the only means of communication or environment control. Locked-in syndrome can be caused, for example, by amyotrophic lateral sclerosis(ALS), brainstem stroke, mitochondrial disease, spinal-cord injury, traumatic-brain injury, and even later-stage cerebral palsy. Despite these sufferers being completely physically paralyzed and unable to speak, they are however, cognitively intact and alert and thus have a need to communicate. It is estimated that in the order of one million people worldwide suffer from locked-in syndrome. It is this motivation that has inspired researchers to explore the possibility of harnessing the intact brain signals of these people as a means of communication.

BCI design represents a new frontier in science and technology that requires multidisciplinary skills from fields such as neuroscience, engineering, computer science,

psychology and clinical rehabilitation to achieve the goal of developing an alternative communication medium. Despite the technological developments, there remain numerous obstacles to building efficient BCIs. The biggest challenges are related to accuracy, speed and usability. Due to these limitations, no BCI system has become commercially available as yet. If a disabled person can move their eyes or even one muscle in a controlled way, the interfaces based on eye-gaze or EMG switch technology are more efficient than any of the BCIs that exist today. The maximum transfer rate of current BCI systems is in the order of 25 bits/min. The standard dial-up modem can transfer information at a rate of 56 kbps and even this is rapidly being replaced by megabit and even gigabit technology. The question that remains to be answered by the scientific community is: what is the future of BCI technology outside rehabilitative communication and control applications for the severely disabled? Can the wider population expect to play games, browse the internet and navigate other multimedia rich applications via thought alone? The research carried out in this thesis explores the field of BCI design and implementation in the hope of understanding the potential of this technology.

## **2.2 History**

The idea of being able to control a device through mere thought is not new. In the scientific world, this idea was proposed by Jacques Vidal in 1973 in an article entitled 'Toward Direct Brain-Computer Communications' [3]. In this article, the Belgian scientist, who had studied in Paris and taught at UCLA, describes the hardware architecture and the processing he sought to implement in order to produce a BCI through electroencephalographic signals. In 1971, Eberhard Fetz had already shown that it was possible to teach a monkey to voluntarily control motor cortex brain activity by providing visual information according to

discharge rate [4]. These two references show that since that time, BCIs could be implemented in the form of invasive or non-invasive brain activity measurements, that is, measurements of brain activity at the neural or scalp levels. For a more comprehensive history of BCIs, the reader may refer to the following articles: [5, 6].

Although BCIs have been present in the field of research for over 40 years, they have only recently come to the media's attention, often described in catchy headlines such as "writing through thought is possible" or "a man controls a robot arm by thinking". Beyond announcements motivated by journalists' love for novelty or by scientists and developers' hopes of attracting the attention of the public and of potential funding sources, what are the real possibilities for BCIs within and outside research labs?

This thesis seeks to pinpoint these technologies somewhere between reality and fiction, and between super-human fantasies and real scientific challenges. It also describes the scientific tools that make it possible to infer certain aspects of a person's mental state by surveying brain activity in real time, such as a person's interest in a given element of his or her environment or the will to make a certain gesture. This thesis also explores patients' expectations and feedback, the actual number of people using BCIs and details the material and software elements involved in the process.

## **2.3 Steps involved in BCI**

### **2.3.1 Data acquisition**

The main purpose of this step is to acquire signals from brain activities using various types of sensors including electroencephalography (EEG), Magnetoencephalography (MEG),



electrocorticography (ECoG), electrical signal acquisition in single neurons (intracortical neural recording - INR), functional magnetic resonance imaging (fMRI), and functional near infrared spectroscopy (fNIRS). These brain data acquisition methods are evaluated by a few different criteria. Typical criteria include manner of deploying sensors, type of acquired signal, temporal resolution which is the ability to detect changes within a certain of time interval [7], spatial resolution which is the ability to detect source of changes in brain, and portability which is the ability to use acquisition device across different environments. Table 2.1 shows a summary comparison of these data acquisition methods based on the above criteria. In thesis our experiments were mainly based on EEG and fNIRS signals.

Method	Activity	Temporal resolution	Spatial resolution	Deployment	Portability
EEG	Electrical	0.05 s	10 mm	Non-invasive	Portable
MEG	Magnetic	0.05 s	5 mm	Non-invasive	Non-portable
<u>ECoG</u>	Electrical	0.003 s	1 mm	Invasive	Portable
INR	Electrical	0.003 s	0.05-0.1 mm	Invasive	Portable
<u>fMRI</u>	Metabolic	1 s	1 mm	Non-invasive	Non-portable
<u>fNIRS</u>	Metabolic	1 s	5 mm	Non-invasive	Portable

Table 2.1: Summary of brain data acquisition methods [8, 9] Method

### 2.3.2 Pre-processing

This step is to clean and de-noise data acquired from the previous step in order to enhance relevant information [10]. Besides the main event the experiments would like to acquire, there are many types of artifacts from both subjects participating in the experiment and the system. The system artifacts are a 50/60 Hz power supply interference, electrical noise from electronic components, and cable defects. The subject artifacts are body- movement related

to electrooculography(EOG), electromyography (EMG), electrocardiography (ECG), and sweating. These artifacts make the recorded EEG signal to have a low signal-to-noise ratio (SNR).

### **2.3.3 Feature extraction**

Feature extraction is a crucial step in the BCI scheme. Its task is to represent the whole signal by using some shorter and more meaningful measures called features [10, 11]. Until now, although there has been a lot of effort from neuroscientists seeking to discover brain and neural operations inside it, the overall knowledge of human-beings about the brain is still very limited. This shortcoming makes brain signal more difficult than other signals such as voice signal in feature extraction.

### **2.3.4 Classification**

The task of the classification step is to assign an object represented by a feature vector to a class. In a BCI system, classes are usually brain states or, subject real or imaginary actions. One of the most important challenges of BCI systems is that, due to difficulties in setting up experiments, sample data used for the training phase is quite small compared with the feature vector size. Thus, trained classifiers are easy to become overfit. Researchers have tried to apply a number of classifiers [11], both linear and non-linear. Some well known and successful methods are Linear Discriminant Analysis (LDA), Principal Component Analysis (PCA), Support Vector Machine (SVM), Hidden Markov Model (HMM), k-nearest neighbours (kNN) and Artificial Neural Network (ANN). Among them, LDA and SVM are the two best classifiers [11].

### 2.3.5 Application interface

After correctly identifying brain state or brain activity, the results of the classifier are converted into some command sets which will be sent to control devices. This step depends on the specific electronic device and application.

### 2.3.6 Feedback

Feedback is the last step helping users control their brain activity and in this way this improve the BCI system's performance. Usually, it provides the user with feedback about brain states. In most BCI systems, the feedback step is used in the training phase or offline phase [12].

An overview of a general BCI system framework is shown in Fig. 2.1

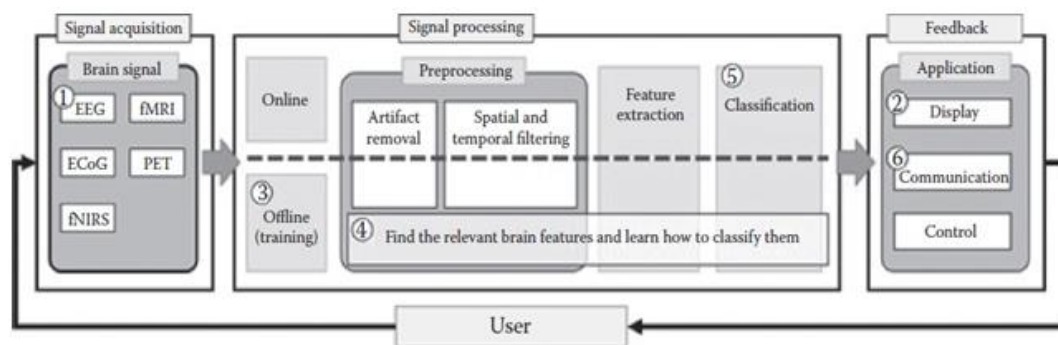


Figure 2.1: Overview of a general BCI system framework

## 2.4 Signal Acquisition Methods

BCIs require a neuroimaging or neurophysiological device to acquire and transmit the brain signals from brain to computer. In general, neuroimaging methods are categorized by invasiveness of the recording methods, but can be further classified by spatial/temporal resolution, direct/indirect measurement, and complexity/price. Each recording technique has strengths, weaknesses, and specific uses that help researchers decide which device is

relevant to their study. Fig 2.2 provides a pictorial classification of BCI systems whereas Fig 2.3 visually compares different recording methods discussed in more detail in the following sections.

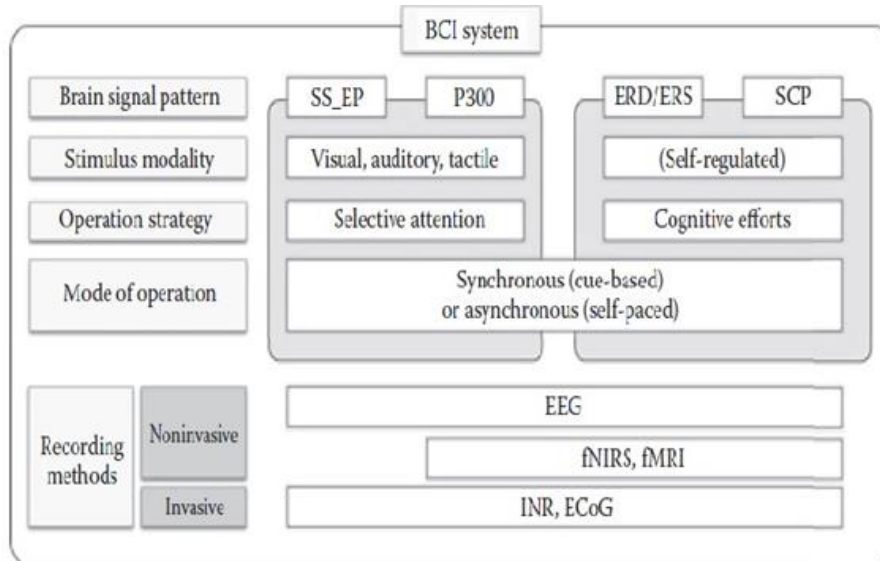


Figure 2.2: classification of BCI systems

## 2.5 Noninvasive Recording Methods

A noninvasive recording technique uses sensors placed on the skin, such as the scalp, or machinery that surrounds the cranium in whole. Two types of noninvasive recording methods discussed in this section include (1) direct measures that detect electrical (e.g., EEG) or magnetic activity (e.g., MEG) of the brain, and (2) indirect measures of brain function reflecting brain metabolism or hemodynamics of the brain (e.g., fMRI, fNIRS, and PET) that do not directly characterize the neuronal activity. Unlike invasive recording methods, these noninvasive techniques do not require surgery, internal chemical or machine implantation, or needle insertion in order to receive and record neural activity [13].

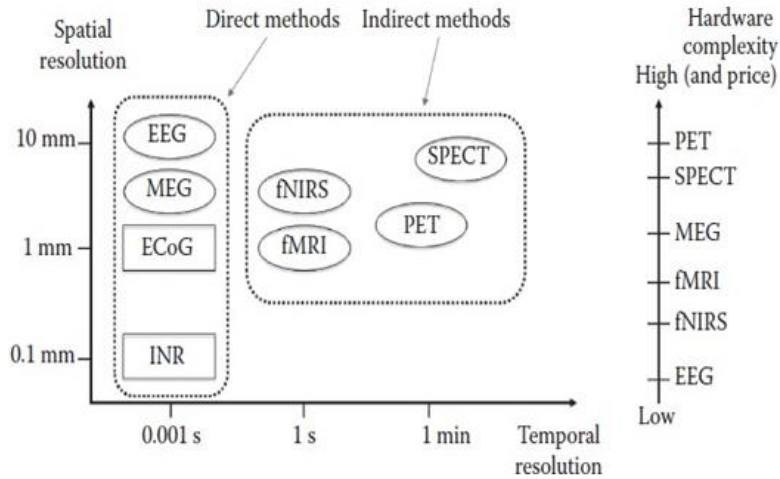


Figure 2.3: Comparison of different signal acquisition methods

### 2.5.1 Electroencephalography

One of the most popular noninvasive neurophysiological recording techniques is electroencephalography, or EEG. This method measures electrical activity in the brain through the use of surface electrodes placed on the scalp [14]. The first human EEG was recorded by Hans Berger, a German psychiatrist, in 1924.

The neurophysiological origin of EEG signals is the pyramidal neurons of the cortex [15]. An electrical impulse is sent down the axon and into the synapse every time neurons are fired during excitation. Since electrical signals are not able to cross neuronal boundaries, a chemical reaction is created between neurons. This chemical reaction is triggered by the electrical impulse and causes an action potential. An action potential is the process of neuron depolarization, followed by repolarization. Chemical information can begin flowing through the synaptic left when a neuron is at its resting polarization level. The flow causes the depolarization, and repolarization is necessary before more chemical information can flow through the synapse again (Nunez 1995). EEG measures the electrical current, which

Teplan explained as “that flow during synaptic excitations of the dendrites of many pyramidal neurons in the cerebral cortex” [16]. Because of the distance and impedance of bone and skin between the electrodes and the cerebral cortex, the EEG cannot accurately detect single neuron excitations. Instead, the EEG picks up local current flows on groups of active neurons within the cerebral cortex [16, 17]

Neural oscillations that are observed in EEG signals are popularly called “brainwaves,” reflecting different aspects when they occur in different locations in the brain Table 1.1. These brain-waves are identified by frequency (in hertz or cycles per second) and amplitude in the range of microvolts ( $\mu\text{V}$  or  $1/1,000,000$  of a volt). Each brainwave has its own set of characteristics representing a specific level of brain activity and mental states [18]. For example, Delta brain-waves reflect slow, loud, and functional mental states that prevail during the late sleep [19], while the power decrease at the alpha band correlates to the presence of mental imagery [20].

In order to record EEG signals, a head set consisting of an EEG cap with at least three electrodes (i.e., a ground, a reference, and a recording electrode) is needed Fig. 2.4b. In addition, an amplifier, an A/D converter, and a computing device (such as a computer) are necessary [9]. Electrodes are typically made of silver, silver chloride, or gold and can be considered wet, which requires conductive gel to be placed between electrode and scalp, or dry, where the electrode is placed directly onto the skin [21, 22]. Measurements from all electrodes are referred to one common electrode, called “reference” electrode [23]. The active and reference electrodes serve as the signal receptors for potential difference comparisons. The ground electrode serves as the baseline of brainwave signals that helps weed out irrelevant data from the active and reference signals.




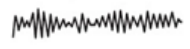


Brainwave	Sample Pattern	Frequency (Hz)	Amplitude ( $\mu V$ )
Delta		0.5-4	100-200
Theta		4-8	5-10
Alpha		8-12	20-80
SMR		12-15	-
Beta		15-25	1-5
Gamma		25-60	0.5-2

Table 2.2: Different Categories of Brainwave Patterns

Correct EEG electrode placement is important to ensure proper location of electrodes in relation to cortical areas so that they can be reliably and precisely maintained from individual to individual. The international 10/20 system has been an internationally recognized standard system for electrode positioning with 21 electrodes for half a century [24, 25]. Under the 10/20 system, the skull is divided into six areas from nasion toinion with interval rates of 10%,20%, 20%, 20%, 20%, and 10% (Fp: pre frontal, F: frontal, C: central, P: parietal, and O: occipital, respectively), and also divided into the same ratios from left to right pre-auricular points (T3: temporal, C3: central, Cz, C4, and T5, respectively) [26]. With the advent of multichannel EEG acquisition systems and the concurrent development of topographic and tomographic signal source localization methods, however, the international 10/20 system has been extended to higher-density electrode settings such as the 10/10 and 10/5 systems, allowing more than 500 electrode positions (for the effectiveness of 10/20-derived systems. Fig. 2.4a and Fig. 2.4b

demonstrate the 10/20 international system of electrode placement and an example montage based on the 10/10 system, respectively. To accurately identify the location of scalp electrodes, anatomical landmarks should be determined for the essential positioning of the electrodes: (1) the nasion, which is the point between the forehead and the nose; (2) the inion, which is the lowest point of the skull from the back of the head and is normally indicated by a prominent bump; (3) the pre-auricular points anterior to the ear. The numbers “10” and “20” refer to the fact that the distances between adjacent electrodes are either 10% or 20% of the total front–back or right–left distance of the skull. Each site has a letter to identify the lobe (i.e., F, T, C, P, and O stand for Frontal, Temporal, Central, Parietal, and Occipital, respectively), the Z(ero) to refer to an electrode placed on the midline, and a number to identify the hemisphere location (i.e., odd and even numbers referring to the left and right hemispheres, respectively). Also note that the smaller the number, the closer the position is to the midline. In Fig. 2.4a for example, electrode O1 identifies the left occipital, C4 identifies the right central, P3 identifies the left parietal, and A1 identifies the left ear reference.

Currently, EEGs are among the most popular techniques for brain–computer



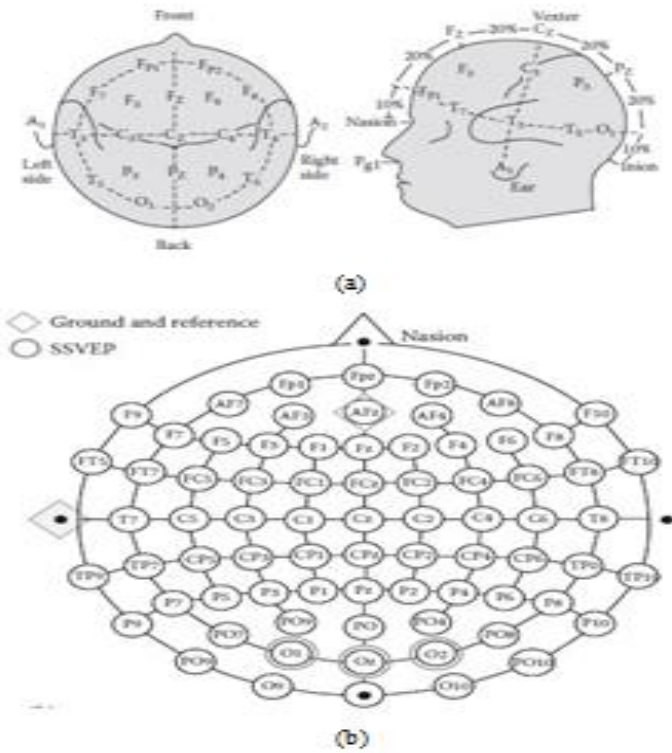


Figure 2.4: (a) The 10/20 international system of electrode placement. (b) An example montage based on the 10/10 system, which measures O1 and O2 with Oz bipolar method to elicit SSVEPs.

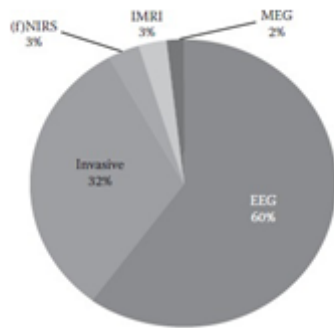


Figure 2.5: BCI research articles [27]

interfacing technology, making up 68% of BCI research articles published in 2007–2011 as shown in Fig. 2.5 [27]. It is noninvasive, inexpensive, and portable, making it a popular device in current research. It does not, however, provide high spatial quality information on the location of brain signal activation. In addition, it is mathematically difficult to accurately compute the distribution of currents within the brain that generated these signals. This is referred to as the “inverse problem” [28].

### **2.5.2 Magnetoencephalography**

MEG is another recording technique for non-invasively measuring the magnetic fields generated by neuronal activity of the brain. When active neurons generate electric currents, a miniscule magnetic field is created [29]. This magnetic field is impossible to detect from the activation of a single neuron, but when many neurons fire together, a larger and more easily detectable magnetic field is created. MEG combines functional information from the magnetic field recordings with structural information from other anatomical images, such as magnetic resonance imaging (MRI).

The hardware required includes the MEG scanner that is equipped with a superconducting quantum interference device or SQUID that was invented in the 1960s as a sensor of magnetic field changes. The principle features of MEG are as follows: (1) a direct measure of brain function, (2) a very high temporal resolution on the order of milliseconds, (3) an excellent spatial resolution with millimeter precision, and (4) a noninvasive method that does not require the injection of isotopes or exposure to x-rays or magnetic fields (Uhlhaas 2015).

Despite MEGs having better spatial resolution and very similar temporal resolution to EEG, they are used less in BCI research—accounting for only 2% of relevant literature (Fig. 2.5).

This is likely due to the non-portability and high cost. In addition, MEG requires highly sensitive instrumentation and sophisticated methods, such as a magnetically shielded room for eliminating environmental magnetic interference [17].

### **2.5.3 Functional Magnetic Resonance Imaging**

Functional magnetic resonance imaging or functional MRI (fMRI) is a noninvasive, functional neuroimaging method that indirectly measures neuronal activity of the brain by identifying the hemodynamic response, known as the blood oxygen level-dependent (BOLD) contrast.

The fMRI principle is based on the so-called neurovascular coupling in which neuronal activation and metabolism with regional cerebral blood flow (rCBF) and regional cerebral blood oxygenation (rCBO) are tightly coupled [31]. When neurons fire, the surrounding blood of the firing neurons experiences a decrease in oxygenated blood, and then a rapid increase in rCBF and oxygen metabolism (cerebral metabolic rate of oxygen, CMRO<sub>2</sub>) as more oxygenated blood and glucose flow to the area for use in energy consumption [32]. The increased oxygen metabolism then converts the oxyhemoglobin in the blood (oxy-Hb) to the deoxygenated blood (deoxy-Hb). On the other hand, a disproportionately large increase in rCBF leads to a washout of deoxy-Hb from the activation area, resulting in a decrease of deoxy-Hb and an increase of oxy-Hb [31]. It has long been suggested that rCBF increases exceed CMRO<sub>2</sub> increases by a factor of 2–10 [33]. Deoxygenated blood transmits greater magnetic fields, interfering with the MRI's magnetic field. However, oxygenated blood creates less intense magnetic fields and therefore interferes with the MRI less, allowing activated neuron areas to be viewable owing to an increase in oxygenated blood flow [34].

fMRI data imagery is shown very close to the blood flow, within approximately 1 mm of accuracy and within approximately 1 s of oxygenated blood flow increase [9]. That is, fMRIs offer highly accurate spatial information that could be very useful for detailed BCI tasks, but their temporal resolution is quite slow compared to techniques such as EEG or MEG. In addition, fMRI does not measure neural activity directly, but allows for inference of neural activity from measured blood volume and blood flow. Other downfalls include size, and expense of use, making them ineffective and impractical for everyday purposes. Research articles discussing fMRI-BCIs accounted for only 2% of the literature (Fig. 2.5).

#### **2.5.4 Functional Near-Infrared Spectroscopy**

Similar to fMRI, functional near-infrared spectroscopy (fNIRS) relies on the changes in oxygenated and deoxygenated blood in the cerebral cortex. Oxygenated and deoxygenated blood absorb light at different rates. For example, deoxygenated blood absorbs more light below 800 nm light, while oxygenated blood does above 800 nm [35, 36]. fNIRS takes advantage of the differences in light absorption to detect neuronal activity.

The hardware required for fNIRS includes an infrared light source, a light detector, signal processing devices, and a computing device such as a computer [9]. Through the use of an infrared light placed on the scalp and a light detection device placed nearby, levels of neuronal activation can be detected. The infrared light penetrates the scalp and bone and the upper level of the cerebral cortex and, depending on the amount of oxygenated or deoxygenated blood in the area, a certain amount of light is allowed to pass through, and some light is reflected back out of the scalp [17]. This penetrating light is identified by the light detector. As discussed in the previous subsection, neuron firings cause oxygenated

blood to rush to the surrounding area, bringing glucose for energy. This shift in blood oxygen levels causes the light to act differently, providing a change in the signal sent to the light detector, which is then processed and recorded.

fNIRS BCIs are not nearly as popular as EEG systems. Research articles focused on fNIRS BCIs accounted for just 3% of the relevant published material (Fig. 2.5). Coyle and colleagues [37] found that fNIRS BCIs can be accurately and simply commanded through motor imagery and proper light and detector placement. Because of the latent nature of the blood flow response to neuron activated sites in the cerebral cortex, the temporal resolution is slower in fNIRS than in EEG or invasive methods. In addition, fNIRS signals are vulnerable to motion and pulse artifacts caused by physical motions and heartbeats during the measurement, respectively [38]. Thus, fNIRS should be pre-processed with elaborate artifact removal methods, such as ICA and wavelet, to improve the signal-to-noise ratio (SNR) before feature extraction. fNIRS is also limited to detecting changes in the surface areas of the brain, as the infrared light can only penetrate so far. It is, however, a portable and inexpensive option, making it a decent candidate for home settings [39].

### **2.5.5 Positron Emission Tomography**

PET is a noninvasive, three-dimensional (3D) radiation or nuclear medicine imaging technique that is used to measure the functional processes within the human body, including neural activity [40]. The PET principle is based on the phenomenon of positron annihilation. That is, when a positron passes through matter, two photons are simultaneously emitted in almost exactly opposite directions. This method relies on a positron-emitting tracer atom that is introduced into the bloodstream in a biologically active

molecule, such as fludeoxyglucose, which acts similarly to glucose in the body. Fludeoxyglucose will concentrate in areas with higher metabolic needs. Over time, this tracer molecule emits positrons, which are detected by a sensor. The spatial location of the tracer molecule in the brain can be determined based on the emitted positrons. This allows researchers to construct a 3D image of the areas of the brain that have the highest metabolic needs, typically those that are most active [41].

In general, the arrangement of a PET machine consists of coincidence detectors, scintillating crystals, and block detectors. However, most BCI research utilizing PET is limited to clinical studies because of its disadvantages, including its high cost and lower half-life of the radionuclide ([13, 42–44]).

## **2.6 Invasive Recording Methods**

Invasive recording methods are neuroimaging techniques in which the electrodes make direct contact with brain tissue. These methods can provide more accurate spatial and temporal information, but come at a greater risk to the individual. Two types of invasive recording methods — electrocorticography (ECoG) and intracortical neuron recording (INR) — are discussed in this section.

### **2.6.1 Electrocorticography**

ECoG is also referred to as intracranial EEG, a method of recording electrical impulses with electrodes that are placed on the brain in order to bypass impeding material such as the scalp and skull. The physiology behind ECoG is the same as that for EEG, but sensitivity in ECoG is greater because of the close nature of the electrodes to the neurons. In order for the

electrodes to be placed on the surface of the cortex, surgery involving removing part of the skull is required. A group of electrodes spaced about 1 cm apart from each other are placed lightly on either the epidural or sub-dural layer of the brain. The spacing and grouping of the electrodes are kept consistent through the use of clear, flexible grid structure. Electrodes can be placed temporarily and patients can complete tasks while cognizant during the surgical procedure or they can be placed permanently for use outside of the operating room. ECoG offers higher temporal [45] and spatial resolution than EEG (e.g., tenths of millimeters vs. centimeters) [46], broader bandwidth (e.g., 0–500 Hz vs. 0–50 Hz) [47], higher characteristic amplitude (i.e., 50–100  $\mu\text{V}$  vs. 10–20  $\mu\text{V}$ ) [23], and far less vulnerability to artifacts such as EMG (Ball et al. 2009) or ambient noise [23]. Leuthardt and colleagues found that users of ECoG BCIs had a quicker training rate than those who used EEG BCIs [48]. Invasive techniques accounted for 32% of the literature over the 2007–2011 period (Figure 2.5). Even still, the invasive nature of ECoG poses obvious risks, including the chance that electrodes can unintentionally move from their initial placement. In addition, patients are also at risk of postoperative infection and tissue reaction [39, 49, 50]. Furthermore, the long-term stability of ECoG signals has not been well researched.

## 2.6.2 Intracortical Neuron Recording

INR is a technique that allows for neuronal activity in the gray matter of the brain to be recorded. Just like the EEG and ECoG, this technique relies on the electrical impulses of the brain. Through the use of a penetrating electrode made of glass, platinum or tungsten, placed near or within a neuron cell body, electrical currents are able to be observed. This technique can be so precise it detects one single neuron, known as single unit activity

(SUA). Or it can be used to detect multiple neuronal impulses, known as multi-unit activity (MUA). Or more generally, INR can identify local field potentials (LFPs), which are the electrical impulses in the surrounding area of the electrode placement [51].

Research into INR began with animal subjects and has since been applied to humans—especially those with severe motor disorders. Coupled with ECoG, research into BCIs using these methods accounted for 32% of the literature (Fig. 2.5). The spatial resolution of INR is very detailed and surpasses all other types of invasive and noninvasive neuroimaging techniques, whether recording SUA, MUA, or LFPs. The temporal resolution is similar to that of ECoG. This method has associated risks, including the diminishing of signal acquisition through the electrode over time, tissue damage, foreign body rejection, or electrode movement within the brain [52].

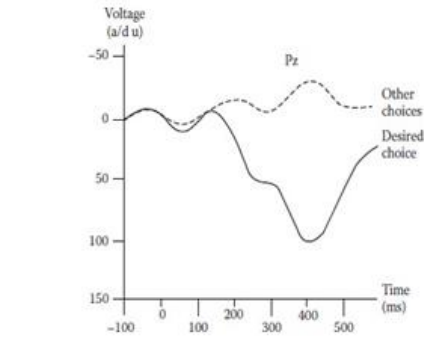
## **2.7 Brain Signal Patterns for BCI Operation**

Every BCI is created to respond to a certain type of brain signal. Fig. 2.6 illustrates the most popular types of brain signals used for operating BCIs. What follows is an overarching review of the brain signal patterns in terms of their physiological bases, initial training requirement for use, and the rate at which information is transferred from brain to application. However, only neuroelectric signals, such as EEG, are discussed in the following sections, because it not only can cover most of brain patterns (P300, SSEP, and ERD/ERS) as shown in Fig. 2.2 but also is the most studied BCI system because of its simplicity in application [14].

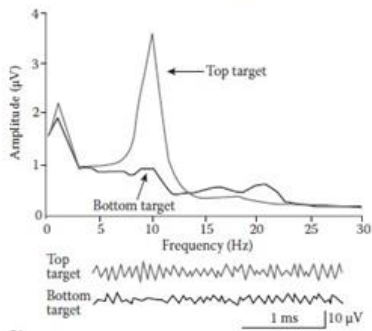


### 2.7.1 P300 ERPs

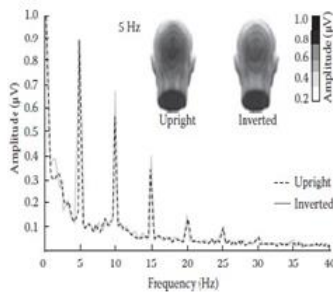
The P300 wave is an ERP component of the EEG that reaches a maximum positive peak in voltage about 300 ms after a stimulus onset (Fig. 2.6a). It is most commonly elicited in an “oddball” paradigm when a subject responds to target stimuli that occur infrequently and irregularly within a series of standard stimuli that occur frequently and regularly [53]. The amplitude of the P300 wave is maximal at central and parietal scalp regions (e.g., Pz), varying with the improbability of the targets. Its latency is proportional to the difficulty of discriminating the target stimulus from the standard stimuli [54]. The stimulus can be visual [56], auditory [57], or even tactile [58]. Since the P300 response to external stimuli is automatic, initial training is not required to teach users to control their brain signals. A short training may be necessary for certain applications using the P300 wave owing to complicated interfaces or for the sake of the classification algorithm. [58] found that healthy individuals were able to achieve high accuracy levels with very little training time. The high levels of accuracy coupled with the low-cost, easy-to-use EEGs used to measure this response make the P300 wave a useful and popular tool for BCIs. P300 BCIs can also provide the user with a large amount of options to choose.



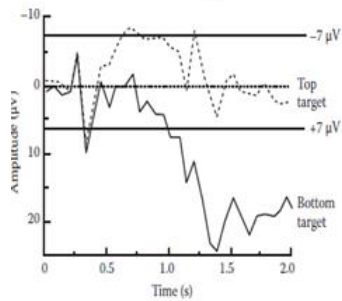
(a)



(b)



(c)



(d)

Figure 2.6: Brain signal patterns for BCI operation. (a) P300 ERP (b) Steady-State Evoked Potentials (c) Sensorimotor Rhythms (d) Slow cortical Potential

## 2.7.2 Steady-State Evoked Potentials

When presented with steady-state (i.e., vibratory in nature) stimuli, the rhythmic brain activity in the associated cortical area will be generated, mimicking the frequency of the stimuli (Fig. 2.6b). The stimulus can be visual, auditory, or even tactile. For example, SSVEPs are currently the most popular choice for brain signals in BCI operations. SSSEPs to be elicited by vibrotactile stimuli [59] and SSAEPs to be elicited by auditory stimuli [60] have also been used in BCI research.

BCIs that use SSVEPs as their control signal usually have lights or other stimuli that flash at differing frequencies. Each light or pattern is linked with a control option (e.g., direction, on/off, etc.) for the BCI application. For example, a 9-Hz flickering light-emitting diode (LED) is for turning on TV, while an 11-Hz LED is for turning off TV. Selections are made through users focusing on whichever stimulus is associated with the action they want to perform. The neuroimaging device records the frequency of the brain signals and interprets the selection. SSVEP BCIs do not require training and provide the quickest and most reliable communication in EEG BCIs [61–63]. However, as SSVEP BCIs required eye gaze and focus, they may not be suitable for users with severe motor disabilities and those who are visually impaired [9]. Moreover, staring for long periods of time at flashing lights or stimulus may also induce fatigue.

### 2.7.3 Sensorimotor Rhythms

SMRs are brainwave patterns recorded in the somatosensory and the motor cortices (Fig. 2.6c). These patterns can change due to either movement or imagined movement. There are two rhythms relevant to SMRs: the Mu band (7–13 Hz, alpha band present in the somatosensory and motor cortices) and the Beta band (14–30 Hz). Real and imagined movement creates what are known as event-related desynchronization (ERD) and event-related synchronization (ERS).

ERD is the decrease in frequency band amplitude in the sensorimotor areas of the brain related to movements or imagined movement. ERS is the increase in frequency band amplitude in the sensorimotor areas immediately after movement or imagined movement [7]. Mu band ERD starts right before movement onset, reaches the maximal ERD shortly after movement onset, and recovers its original level within a few seconds. In contrast, the beta band shows a short ERD during the initiation of movement, followed by ERS that reaches the maximum after movement execution. This ERS occurs when the Mu rhythm is still attenuated [9]. In order for the signal emitting from these movements or imagined movements to be strong enough, the area of usage in the brain needs to be large enough. The hands, feet, and tongue are represented over large areas of the somatosensory and motor cortices owing to the complex and regular motion they produce. BCIs using SMRs often use the imagined movement of feet, hands, or tongue for the purposes of control [7]. Since outside stimulation is not required for this BCI type, and the brainwaves and interactions with the BCI are controlled by thought processes, training—sometimes extensive training—is required, employing techniques such as operant conditioning.

### **2.7.4 Slow Cortical Potentials**

Generalized changes in the polarization levels of superficial cortical neurons are known as slow cortical potentials (SCPs) [64]. A change in the direction of negative polarity is associated with increased cortical activity or movement, while a change in the direction of positive polarity is associated with decreased cortical activity and calm (Fig. 2.6d). SCPs are generally analyzed through the Thought Translation Device. Extensive and intensive training is required, using individualized cognitive and behavioral strategies [65]. SCPs take anywhere from 1 s to several seconds to develop, and therefore the information transfer rate is quite slow compared to SSVEP and visual P300, which does not allow for much efficiency in use. Similar to SMR BCIs, SCP BCIs do not rely on external stimulus such as visual stimuli of SSVEP in order to elicit brainwave patterns to use to influence the interface. Instead, users control their thought processes in order to interact with the BCI.

### References

1. J.R. Wolpaw, et al., "Brain-computer interface technology: a review of the first international meeting," in IEEE Transactions on Rehabilitation Engineering, vol. 8, no. 2, pp. 164-173, June 2000.
2. J.J. Vidal, "Real-time detection of brain events in EEG," in Proceedings of the IEEE, vol. 65, no. 5, pp. 633-641, May 1977.
3. J.J. Vidal, "Toward direct brain-computer communication", Annual Review of Biophysics and Bioengineering, vol. 2, no. 1, pp. 157-180, 1973.
4. E.E. Fetz and D.V. Finocchio, "Operant conditioning of specific patterns of neural and muscular activity", Science, vol. 174, 1971.
5. M. Lebedev and M. Nicholelis, "Brain-machine interfaces: past, present and future", Trends in Neurosciences, vol. 29, no. 9, pp. 536-546, 2006.
6. E. Vaadia and N. Birbaumer, "Grand challenges of Brain-Computer Interfaces in the years to come", Frontiers in Neuroscience, vol. 3, no. 2, pp. 151-154, 2009.
7. B. Graimann, et al., "Brain-Computer Interfaces: A Gentle Introduction", Brain-Computer Interfaces. The Frontiers Collection. Springer, Berlin, Heidelberg, 2010
8. H. Gu'rk'ok and A. Nijholt, "Brain-Computer Interfaces for Multimodal Interaction: A Survey and Principles", International Journal of Human-Computer Interaction, 28:5, pp. 292-307, 2012
9. L. F. Nicolas-Alonso and J. Gomez-Gil, "Brain Computer Interfaces, a Review," Sensors, vol. 12, no. 2, pp. 1211-1279, Jan. 2012.
10. A. Bashashati, M. Fatourechi, R.K. Ward, and G.E. Birch, "A survey of signal processing algorithms in brain-computer interfaces based on electrical brain signals", Journal of Neural engineering, vol. 4, no. 2, 2007.
11. F. Lotte, M. Congedo, A. L'ecuyer, F. Lamarche, and B. Arnaldi, "A review of classification algorithms for EEG-based brain-computer interfaces", Journal of Neural Engineering, vol. 4, no. 2, 2007.

12. F. Lotte, C. Guan and K.K. Ang, "Comparison of designs towards a subject-independent brain-computer interface based on motor imagery," 2009 Annual International Conference of the IEEE Engineering in Medicine and Biology Society, Minneapolis, MN, 2009, pp. 4543-4546.
13. S. Bhattacharyya, "A review on brain imaging techniques for BCI applications", Biomedical Image Analysis and Mining Techniques for Improved Health Outcomes, 39, 2015.
14. E. Niedermeyer, and F.L. da Silva, Electroencephalography: Basic Principles, Clinical Applications, and Related Fields, vol. 1, 2005.
15. D.S. Cantor and J.R. Evans, Clinical Neurotherapy: Application of Techniques for Treatment, Academic Press, 2013.
16. M. Teplan, "Fundamentals of EEG measurement", Measurement Science Review, 2(2), 2002.
17. O. Tonet, et al., "Critical review and future perspectives of non-invasive brain-machine interfaces", Journal of Neuroscience Methods, 31(0), 2006.
18. C. Muhl, et al., "A survey of affective brain computer interfaces: Principles, state-of-the-art, and challenge." Brain-Computer Interfaces, 1(2), pp. 66-84, 2014.
19. M. Steriade, et al., "Thalamocortical oscillations in the sleeping and aroused brain", Science, 262, 679, 1993.
20. G. Pfurtscheller, "Quantification of ERD and ERS in the time domain", Handbook of Electroencephalography and Clinical Neuropsychology, Event-Related Desynchronization, vol. 6, pp. 89-105, Amsterdam: Elsevier, 1999.
21. H.L. Peng, et al., "Flexible dry electrode based on carbon nanotube/polymer hybrid micropillars for biopotential recording. Sensors and Actuators A: Physical, 235, pp. 48-56, 2015.
22. H.L. Peng, et al., "A novel passive electrode based on porous Ti for EEG recording", Sensors and Actuators B: Chemical, 226, pp. 349-356, 2016.
23. G. Schalk and J. Mellinger, "A Practical Guide to Brain-Computer Interfacing with BCI2000: General Purpose Software for Brain-Computer Interface Research, Data Acquisition, Stimulus Presentation, and Brain Monitoring", Springer Science & Business Media, 2010.

24. R.W. Homan, R. W., et al., "Cerebral location of international 10–20 system electrode placement", *Electroencephalography and Clinical Neuro- physiology*, 66(4), pp. 376–382, 1987.
25. H.H. Jasper, "The 10/20 international electrode system", *EEG and Clinical Neurophysiology*, 10, pp. 371–375, 1958.
26. G. Klem, G., et al., "The ten-twenty electrode system of the International Federation", *Electroencephalography and Clinical Neurophysiology*, 10(2), pp. 371–375, 1958.
27. H.J. Hwang, et al., "EEG-based brain–computer interfaces: A thorough literature survey", *International Journal of Human–Computer Interaction*, 29(12), pp. 814–826, 2013.
28. S. Castan˜o-Candamil, et al., "Solving the EEG inverse problem based on space-time-frequency structured sparsity constraints", *NeuroImage*, 118, pp. 598–612, 2015.
29. M. Ha˜ma˜la˜inen, et al., "Magnetoencephalography—Theory, instrumenta- tion, and applications to noninvasive studies of the working human brain", *Reviews of Modern Physics*, 65(2), pp. 413–97, 1993.
30. P. Uhlhaas, "Magnetoencephalography as a tool in cognitive neuroscience: A translational perspective", *Schizophrenia Bulletin*, 41, pp. S98–S99, 2015.
31. U. Lindauer, U., et al. "No evidence for early decrease in blood oxygena- tion in rat whisker cortex in response to functional activation", *Neuroim- age*, 13, pp. 988–1001, 2001.
32. A.K. Dunn, et al., "Spatial extent of oxygen metabolism and hemo- dynamic changes during functional activation of the rat somatosensory cortex", *Neuroimage*, 27, pp. 279–290, 2005
33. A.L. Lin, "No evaluation of MRI models in the measurement of CMRO<sub>2</sub> and its relationship with CBF", *Magnetic Resonance in Medicine*, 60(2), pp. 380–389, 2008.
34. N. Weiskopf, et al., "Principles of a brain–computer interface (BCI) based on real-time functional magnetic resonance imaging (fMRI)", *Biomedical Engineering, IEEE Transactions on*, 51(6), pp. 966–970, 2004.
35. M.E. Giardini, et al., "Portable microcontroller-based instrument for near infrared spectroscopy", *SPIE*, 3911, pp. 250–255, 2000.
36. T. Wilcox, et al., "Hemodynamic response to featural changes in the occipital and inferior temporal cortex in infants: A preliminary method- ological exploration: Paper",



- Developmental Science, 11(3), pp. 361–370, 2008.
37. S.M. Coyle, et al., “Brain–computer interface using a simplified functional near-infrared spectroscopy system”, *Journal of Neural Engineering*, 4(3), pp. 219–226, 2007.
  38. F. Matthews, et al., “Hemodynamics for brain–computer interfaces. *IEEE Signal Processing Magazine*, 25(1), pp. 87–94, 2008.
  39. T. Castermans, et al., “Towards effective non-invasive brain–computer interfaces dedicated to gait rehabilitation systems”, *Brain Sciences*, 4, pp. 1–48, 2014.
  40. J. Stollfuss, et al., “Non-invasive imaging of implanted peritoneal carcinomatosis in mice using PET and bioluminescence imaging”, *EJNMMI Research*, 5(1), pp. 1–8, 2015.
  41. D.W. Townsend, “Dual-modality imaging: Combining anatomy and function”, *Journal of Nuclear Medicine*, 49(6), pp. 938–955, 2008.
  42. H. Boecker, et al., “AH 2 15 O positron emission tomography study on mental imagery of movement sequences—The effect of modulating sequence length and direction”, *NeuroImage*, 17(2), pp. 999–1009, 2002.
  43. S.T. Grafton, et al., Heidelberg, 2010 “Localization of grasp representations in humans by positron emission tomography”, *Experimental Brain Research*, 112(1), pp. 103–111, 1996.
  44. C.J. Winstein, et al., “Motor task difficulty and brain activity: Investigation of goal-directed reciprocal aiming using positron emission tomography”, *Journal of Neurophysiology*, 77(3), pp. 1581–1594, 1997.
  45. C. Henle, et al., “Towards electrocorticographic electrodes for chronic use in BCI applications”, *Towards Practical Brain–Computer Interfaces SE - 5*, pp. 85–103, Springer Berlin Heidelberg, 2013.
  46. W.J. Freeman, et al., “Spatial spectra of scalp EEG and EMG from awake humans. *Clinical Neurophysiology*, 114(6), pp. 1053–1068, 2003.
  47. R.J. Staba, et al., “Quantitative analysis of high frequency oscillations (80–500 Hz) recorded in human epileptic hippocampus and entorhinal cortex”, *Journal of Neurophysiology*, 88(4), pp. 1743–1752, 2002.
  48. E.C. Leuthardt, et al., “A brain–computer interface using electrocorticographic signals in humans. *Journal of Neural Engineering*, 1(2), pp. 63–71, 2004.

49. J.J. Daly, and R.J. Wolpaw, "Brain-computer interfaces in neurological rehabilitation", *The Lancet Neurology*, 7(11), pp. 1032–1043, 2008.
50. C.S. Mestais, et al., "WIMAGINE: Wireless 64-channel ECoG recording implant for long term clinical applications", *IEEE Transactions on Neural Systems and Rehabilitation Engineering*, 23(1), pp. 10–21, 2015.
51. M.L. Homer, et al., "Implants and decoding for intracortical brain computer interfaces", *Annual Review of Biomedical Engineering*, 15, pp. 383–405, 2013.
52. B. Gunasekera, et al. "Intracortical recording interfaces: Current challenges to chronic recording function", *ACS Chemical Neuroscience*, 6(1), pp. 68–83, 2015.
53. A.A. Huettel, and G. McCarthy, "What is odd in the oddball task?", *Neuropsychologia*, 42(3), pp. 379–386, 2004
54. T.W. Picton, "The P300 wave of the human event-related potential", *Journal of Clinical Neurophysiology: Official Publication of the American Electroencephalographic Society*, 9(4), pp. 456–479, 1992
55. C. Bledowski, et al., "Localizing P300 generators in visual target and distractor processing: A combined event-related potential and functional magnetic resonance imaging study" *Journal of Neuroscience*, 24(42), pp. 353–9360, 2004.
56. Musiek, et al., "The auditory P300 at or near threshold, " *Journal of the American Academy of Audiology*, 16(9), pp. 698–707, 2005.
57. A.M. Brouwer and J.B. Van Erp, "A tactile P300 brain-computer interface", *Frontiers in Neuroscience*, 4(19), 2010.
58. C. Guger, et al., "How many people are able to control a P300-based brain-computer interface (BCI)?" *Neuroscience Letters*, 462, pp. 94–98, 2009
59. M. Severens, et al., "Transient and steady-state responses to mechanical stimulation of different fingers reveal interactions based on lateral inhibition. *Clinical Neurophysiology: Official Journal of the International Federation of Clinical Neurophysiology*, 121(12), 2090–6, 2010
60. N.J. Hill, and B. Schalkopf, "An online brain-computer interface based on shifting attention to concurrent streams of auditory stimuli", *Journal of Neural Engineering*, 9(2), 26011, 2012.

61. I. Volosyak, “SSVEP-based Bremen-BCI interface—Boosting information transfer rates”, *Journal of Neural Engineering*, 8(3), 36020, 2011.
62. Wang, Y., et al., “Brain–computer interfaces based on visual evoked potentials: Feasibility of practical system designs”, *IEEE Engineering in Medicine and Biology Magazine: The Quarterly Magazine of the Engineering in Medicine & Biology Society*, 27(5), pp. 64–71, 2008
63. D. Zhu, et al., “A survey of stimulation methods used in SSVEPbased BCIs”, *Computational Intelligence and Neuroscience*, 2010.
64. U. Strehl, et al., “Sustained reduction of seizures in patients with in- tractable epilepsy after self-regulation training of slow cortical poten- tials—10 years after”, *Frontiers in Human Neuroscience*, 8(604), 1–7, 2010
65. P. Studer, et al., “Slow cortical potential and theta/beta neurofeedback training in adults: Effects on attentional processes and motor system excitability”, *Frontiers in Human Neuroscience*, 8(July), 555, 2014

# Chapter 3

## Fuzzy Chemistry and Fuzzy pH controller

### 3.1 Introduction

Fuzzy theory allows the separation axiom scheme of set theory to be extended to predicates to which a precise truth value cannot be assigned and the membership is nothing but the way for specifying the predicate. In this view, fuzzy theory is certainly a "high" theory allowing the extension of classical logic to fuzzy logic.

Actually, even in high disciplines like physics there are situations of this kind (e.g., statistical and quantum mechanics), but they are more appropriately managed in terms of probability distributions whose features or evolutions are assigned by physical laws. The major advantage of fuzzy theory, the freedom in specifying the memberships, is not useful in these cases that perhaps explains why it has had few applications in these domains.

At the current level of knowledge, chemistry may be viewed as a special

chapter of physics devoted to the description of atomic assemblies (molecules, radicals,...) in terms of their constituting nuclei and electrons in mutual interaction. It is generally believed that a description of molecules in terms of properties of their atomic constituents (general chemistry) is impossible.

This fact is especially disappointing because general chemistry has long reach and large predictive power, even using the limited mathematical apparatus of college algebra; this advantage is especially appreciated when its mathematical apparatus is compared with that involved in the quantum mechanical description of molecules considered as formed by nuclei and electrons extremely complex and requiring heavy calculations on large computers.

The logical structure of a formal theory of general chemistry, where the properties of all molecules are deduced from those of the constituting atoms and bonds (whose properties are assigned a priori), has been constructed. This theory, however, admits the material world as a model ("the theory represents the reality") only if its mathematical structure is based on fuzzy arithmetics. In this way fuzzy logic enters as the basic element of foundational theory like chemistry, rather than simply a tool to manage poorly defined situations.

In this chapter we first introduce the concept of fuzzy logic in chemistry and then discuss in details its applicability in computing chemical properties of atoms, chirality of compounds, and finally the design of fuzzy-controller based on dynamical approach for the calculation of the pH of a chemical reaction/system.

## 3.2 Fuzzy Chemistry

All aspects of molecular shape and size are fully reflected by the molecular electron density distribution [2]. A molecule is an arrangement of atomic nuclei surrounded by a fuzzy electron density cloud. Within the Born-Oppenheimer approximation, the location of the maxima of the density function, the actual local maximum values, and the shape of the electronic density distribution near these maxima are fully sufficient to deduce the type and relative arrangement of the nuclei within the molecule. Consequently, the electronic density itself contains all information about the molecule. As follows from the fundamental relationships of quantum mechanics, the electronic density and, in a less spectacular way, the nuclear distribution are both subject to the Heisenberg uncertainty relationship. The profound influence of quantum-mechanical uncertainty at the molecular level raises important questions concerning the legitimacy of using macroscopic analogies and concepts for the description of molecular properties [3].

Fuzzy set methods have been developed for a variety of applications, initially mostly in engineering and technology [4-11]. However, many applications in the natural sciences quickly followed [12-28]. The Heisenberg relationship and many other aspects of quantum mechanics can be interpreted in terms of fuzzy sets. A straightforward extension of these ideas to some of the elementary concepts of chemistry suggests the following rather natural, fuzzy set representations :

- Molecular nuclear configurations within the nuclear configuration space and potential energy hypersurface model of conformational changes and chemical reactions [17][18] in particular, the distribution and represen-

tation of symmetry domains in the nuclear configuration space, [19] as well as reaction mechanisms [18][20]

- Molecular symmetry and quasisymmetry, using the syntopy model and related approaches [21-24]
- Fuzzy clustering of protein structural classes [25]
- Molecular chirality [26] and various other, more general symmetry deficiencies [27]
- Electron density and related fuzzy Hausdorff distance problems [28],[29]
- Various more general molecular shape problems [30]-[40]

In some of the preceding representations, a natural interrelationship between fuzziness and resolution is used, leading to resolution-based chirality, symmetry and similarity measures. [1], [27]

Both global and local shape properties of molecules can be described using a fuzzy set formalism. This approach is suitable for the description of various functional groups, the local shape changes induced within various molecular moieties by the rest of the molecule, and some effects of shape and shape changes on chemical reactivity. In particular, the density domain approach to chemical bonding [35-36] provides a quantum-chemical, topological description of functional groups and a consistent framework for a detailed shape characterization of global and local features of molecules.

More recently, fuzzy electron density modeling of large molecules have been improved to a level comparable to that achieved earlier for small molecules. The additive fuzzy density fragmentation (AFDF) scheme of Mezey was

described in a general form earlier. [36-37] The simplest version of this scheme, the Mulliken-Mezey AFDF method, is the basis of the molecular electron density lego assembler (MEDLA) technique of Walker and Mezey for generating ab initio quality electron densities for macromolecules. [41-47] The MEDLA method can be applied, virtually without any size limitation, to truly large molecules. This newly available option provided by the MEDLA technique extends the scope of the shape group method to ab initio quality electron density shape analysis of proteins and supramolecular structures.

In this chapter however, we limit our discussion on fuzzy chemistry to defining membership functions for atomic radius, bond length, bond energy, and molecular chirality.

### 3.3 Membership Functions in Fuzzy Chemistry

In the natural interpretation of FC theory,  $C$  is the set of adducts (i.e., any combination of bound atoms), and the molecular graphs (the terms of sort GR satisfying the predicate M) are interpreted as molecules. Whereas,  $Y$  is the set  $F(R)$  of fuzzy numbers defined on  $RLL$ , and the symbols  $+$ ,  $,\dots$  are interpreted as the usual operators of fuzzy arithmetic [5]. Actually the axioms of formal chemistry requires that the quantities of the theory must be added and may be compared with 0. These properties suggest their belonging to an ordered field. The most spontaneous choice, the real space  $R$ , is however not satisfactory because with this assumption formal chemistry does not admit the world of real molecules as a model. Rather, real-world chemistry is a model of



formal chemistry if the quantities of formal chemistry are memberships rather than reals; from this the choice of  $F(R)$  as  $S$ . Any function  $X : GRI \rightarrow NU$  is interpreted as a function that associates fuzzy quantities with molecules:  $I(O) : '10 P \rightarrow *$  The shape of the membership function describing the fuzzy numbers can be different for different functions. In particular for some functional symbol (like  $m$ ) it boils down to singleton characteristic function (i.e. to crisp numbers). Table I summarizes the correspondence between objects of FC theory and of its natural interpretation. The axiom allows defining the mass, energy,... of a molecule starting from the properties of the building blocks: atoms and bonds (which are the natural interpretation of balls and sticks respectively). It is stressed that the fuzziness of formal chemistry is not related to the fact that the quantities of real chemistry may have a statistical distribution. Limiting for simplicity to the internuclear distance, it is well known that the separation between two mutually bonded atoms has a statistical distribution due to the interaction with the thermal embedding (or even to the zero-point vibration). Fuzziness however, does not refer to this distribution; rather it takes into account of the fact that the average separation between two assigned atoms in different molecules varies from one molecule to another. 12 Given the molecules  $A$ ,  $B$  and  $C$ , we read " $A \cup B = C$ " as " $A$  reacts with  $B$  to produce  $C$ " 13 A concrete interpretation of the axioms would require to specify all the parameters of the membership function of the fuzzy numbers used to describe the properties of atoms and bonds. In this paper we simply give some examples of these values, leaving the complete description to future (wider) works.

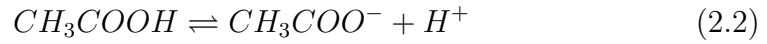
To give an example of the application of FC, we show how to predict the

heat generated by the following chemical reaction:  $H_2 + F_2 \rightarrow 2HF$ . The atoms involved in this reaction are H (hydrogen) and F (fluorine). They are the interpretation (in the natural model) of the balls  $b = (1, 1, 0, 0)$  and  $b_f = (2, 7, 0, 0)$ , respectively. Note that, as shown in Figure 3, the transition from the bag of molecules  $H_2, F_2$  to the bag of molecules  $HF, HF$  is an allowed one. The properties of these atoms are summarized in Table II, where the indicated values are taken from [1]. In the model, the values of atomic radius, self-energy and electronegativity are used as centers of the Gaussian fuzzy numbers that interpret symbols  $r(b_i)$  (see Figure 4, up),  $e(b_i)$  (see Figure 5, up) and  $g(b_i)$ , where  $i \in \{1, 9\}$ . The standard deviations of these Gaussian fuzzy numbers are simply defined as 2 of their centers. Whereas 10 atomic weight are used as crisp values (or Gaussian fuzzy numbers with standard deviation equal to 0) that interpret symbols  $m(b_i)$ . From Axiom FC5 and Definition 7, to compute the energy change  $A_e$  of a reaction we need to compute the energy of each bond involved in it. This is accomplished by using the values of self-energy and electronegativity of the atoms forming the bond, as indicated in Axiom FC3. In the reaction (2) the bonds to consider are H-H, F-F, and H-F; their properties, computed from the properties of composing atoms, are summarized in Table III. Figure 5 shows the self-energies of H and F, the bond energies of H-H, F-F and F-H, and the  $A_e$  of the reaction  $H_2 + F_2 \rightarrow 2HF$ . The vertical line in the lower panel represents the heat of reaction of the reaction. The energy change  $A_e$  is a Gaussian number (whose center can be obtained following Table IV, upper panel), while the heat of reaction is a crisp value calculated as in lower panel of Table IV. The value of the heat of reaction belong to the support of the fuzzy number  $A_e$ . Thus, this

example shows that by using the 'rules' defined by the axioms and simple fuzzy arithmetic it is possible to forecast the heat of reaction. At last, since  $A \in \mathcal{I}$ , from Axiom FC7 it follows that  $H_2 \text{ F}_2 \rightarrow \text{HF}$ .

## 3.4 Fuzy pH controller

### 3.4.1 Dynamic Approach for pH calculation



$$\frac{d[\text{NaOH}]}{dt} = -k_{1f}[\text{NaOH}] + k_{1b}[\text{Na}^+][\text{OH}^-] \quad (2.3a)$$

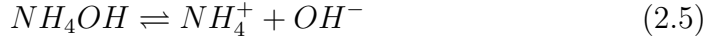
$$\frac{d[\text{Na}^+]}{dt} = k_{1f}[\text{NaOH}] - k_{1b}[\text{Na}^+][\text{OH}^-] \quad (2.3b)$$

$$\frac{d[\text{CH}_3\text{COOH}]}{dt} = -k_{2f}[\text{CH}_3\text{COOH}] + k_{2b}[\text{CH}_3\text{COO}^-][\text{H}^+] \quad (2.3c)$$

$$\frac{d[\text{CH}_3\text{COO}^-]}{dt} = k_{2f}[\text{CH}_3\text{COOH}] - k_{2b}[\text{CH}_3\text{COO}^-][\text{H}^+] \quad (2.3d)$$

$$\frac{d[\text{H}^+]}{dt} = k_{wf} - k_{wb}[\text{H}^+][\text{OH}^-] + k_{2f}[\text{CH}_3\text{COOH}] - k_{2b}[\text{CH}_3\text{COO}^-][\text{H}^+] \quad (2.3e)$$

$$\frac{d[\text{OH}^-]}{dt} = k_{wf} - k_{wb}[\text{H}^+][\text{OH}^-] + k_{1f}[\text{NaOH}] - k_{1b}[\text{Na}^+][\text{OH}^-] \quad (2.3f)$$



$$\frac{d[HCl]}{dt} = -k_{3f}[HCl] + k_{3b}[H^+][Cl^-] \quad (2.6a)$$

$$\frac{d[Cl^-]}{dt} = k_{3f}[HCl] - k_{3b}[H^+][Cl^-] \quad (2.6b)$$

$$\frac{d[NH_4OH]}{dt} = -k_{2f}[NH_4OH] + k_{2b}[NH_4^+][OH^-] \quad (2.6c)$$

$$\frac{d[NH_4^+]}{dt} = k_{2f}[NH_4OH] - k_{2b}[NH_4^+][OH^-] \quad (2.6d)$$

$$\frac{d[H^+]}{dt} = k_{wf} - k_{wb}[H^+][OH^-] + k_{3f}[HCl] - k_{3b}[H^+][Cl^-] \quad (2.6e)$$

$$\frac{d[OH^-]}{dt} = k_{wf} - k_{wb}[H^+][OH^-] + k_{2f}[NH_4OH] - k_{2b}[NH_4^+][OH^-] \quad (2.6f)$$

### 3.4.2 pH Controller Design

In this part, we work on the implementation of a fuzzy controller where we regulate the pH concentration of the solution using a strong acid or strong base in weak base or weak acid medium respectively. In this case, we use the acid HCl and the alkali NH<sub>4</sub>OH to find the suitable pH value.

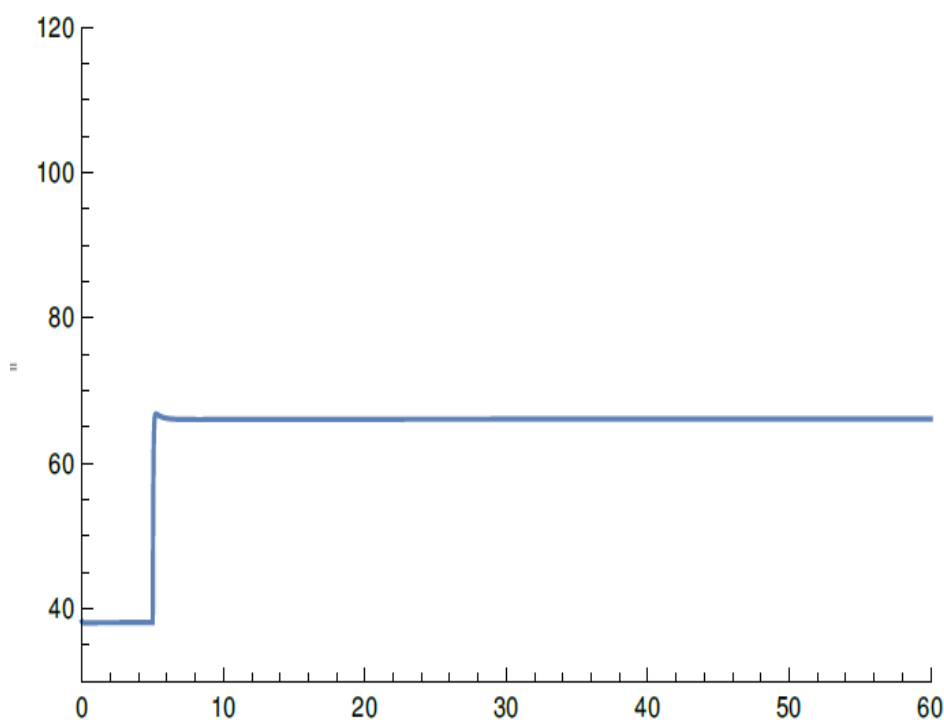


Figure 2.1: pH-Controller

Since it is difficult to find out the transfer function from the dynamics of the system given by the chemical equilibrium differential equations, we can use a Mamdani or Takagi-Sugeno Fuzzy Controller for our system.

From the above equations we see that the variations of the concentrations of  $[H^+]$  and the  $[OH^-]$  with the varying concentration of HCl and  $NH_4OH$ . Now since our optimal pH value is given as 7,  $[H^+] = 10^{-7} = 5.011 \times 10^{-8}$ , and the rate of change of pH should be ideally zero in a stable control system, thus we have to take into the account the case When  $x_1$  is small and large and  $x_2$  is zero.

## 3.5 Conclusion

Through this chapter we were able to implement the concepts of fuzzy logic in different aspects of chemistry.

# Bibliography

- [1] . P. G. Mezey, Shape in Chemistry: An Introduction to Molecular Shape and Topology. VCH, New York, 1993.
- [2] R. G. Woolley, Adv. Phys. 25, 27 (1976).
- [3] L. A. Zadeh, Inform. Control 8, 338 (1965).
- [4] L. A. Zadeh, J. Math. Anal. Appl. 23, 421 (1968).
- [5] A. Kaufmann, Introduction h la Thdorie des Sous-Ensembles Flous. Masson, Paris, 1973.
- [6] M. L. Puri and D. A. Ralescu, J. Math. Anal. Appl. 114, 409 (1986).
- [7] D. Dubois and H. Prade, "Evaluation of Fuzzy Sets and Fuzzy Integration: A Synthetic Discussion," in Abstracts of the Second Joint IFSA-EF and EURO-WG Workshop, pp. 131-135, 1986.
- [8] H. Bandemer and W. N ither, Fuzzy Data Analysis. Kluwer Academic, Dordrecht, 1992.
- [9] E. Sanchez and M. M. Gupta (eds.), Fuzzy Information, Knowledge Representation and Decision Analysis. Pergamon, Elmsford, NY, 1983.

- [10] Z. Wang and G. J. Klir, *Fuzzy Measure Theory*. Plenum, New York, 1992.
- [11] G.J. Klir and B. Yuan, *Fuzzy Sets and Fuzzy Logic, Theory and Applications*. Prentice-Hall, Englewood Cliffs, NJ, 1995.
- [12] E. Prugovecki, *Found. Phys.* 4, 9 (1974).
- [13] E. Prugovecki, *Found. Phys.* 5, 557 (1975).
- [14] E. Prugovecki, *J. Phys. A* 9, 1851 (1976).
- [15] S. T. Ali and H. D. Doebner, *J. Math. Phys.* 17, 1705 (1976).
- [16] S. T. Ali and E. Prugovecke, *J. Math. Phys.* 18, 219 (1977).
- [17] P. G. Mezey, "Topological Model of Reaction Mechanism," in *Structure and Dynamics of Molecular Systems* (R. Daudel, J.-P. Korb, J.-P. Lemaistre, and J. Maruani, eds.), Vol. 1, pp. 57-70. Reidel, Dordrecht, 1985. 5 Fuzzy Measures of Molecular Shape and Size 22]
- [18] P. G. Mezey, *Potential Energy Hypersurfaces*. Elsevier, Amsterdam, 1987.
- [19] P. G. Mezey, *Potential Hypersurfaces*, pp. 187, 364. Elsevier, Amsterdam, 1987.
- [20] P. G. Mezey, "From Geometrical Molecules to Topological Molecules: A Quantum Mechanical View," in *Molecular Organization and Engineering* (J. Maruani, ed.), Vol. 2, p. 61. Kluwer Academic, Dordrecht, 1988.
- [21] J. Maruani and P. G. Mezey, *C. R. Acad. Sci. Paris S r. H* 305, 1051 (1987); 306, 1141 (1987).



- [22] P. G. Mezey and J. Maruani, *Mol. Phys.* 69, 97 (1990).
- [23] J. Maruani and P. G. Mezey, *J. Chim. Phys.* 87, 1025 (1990).
- [24] P. G. Mezey and J. Maruani, *Int. J. Quantum Chem.* 45, 177 (1993).
- [25] C.-T. Zhang, K.-C. Chou, and G. M. Maggiora, *Protein Eng.* 8, 425 (1995).
- [26] P. G. Mezey, "A Global Approach to Molecular Chirality," in *New Developments in Molecular Chirality* (P. G. Mezey, ed.). Kluwer Academic, Dordrecht, 1991.
- [27] P. G. Mezey, *J. Math. Chem.* 11, 27 (1992).
- [28] P. G. Mezey, *Advances in Molecular Similarity* 1, (1996).
- [29] P. G. Mezey, unpublished.
- [30] P. G. Mezey, *Int. J. Quantum Chem., Quantum Biol. Symp.* 12, 113 (1986).
- [31] P. G. Mezey, *Int. J. Quantum Chem., Quantum Biol. Symp.* 14, 127 (1987).
- [32] P. G. Mezey, *J. Comput. Chem.* 8, 462 (1987).
- [33] P. G. Mezey, "Molecular Surfaces," in *Reviews in Computational Chemistry* (K. B. Lipkowitz and D. B. Boyd, eds.), Vol. 1, pp. 265-294. VCH, New York, 1990.
- [34] P. G. Mezey, *J. Chem. Inf. Comput. Sci.* 32, 650 (1992).

- [35] P. G. Mezey, *Canad. J. Chem.* 72, 928 (1994).
- [36] P. G. Mezey, "Density Domain Bonding Topology and Molecular Similarity Measures," in *Topics in Current Chemistry: Molecular Similarity* (K. Sen, ed.), Vol. 173, pp. 63-83. Springer-Verlag, Berlin, 1995.
- [37] P. G. Mezey, "Methods of Molecular Shape-Similarity Analysis and Topological Shape Design," in *Molecular Similarity in Drug Design* (P. M. Dean, ed.), pp. 241-268. Chapman & Hall, London, 1995.
- [38] P. G. Mezey, "Molecular Similarity Measures for Assessing Reactivity," in *Molecular Similarity and Reactivity: From Quantum Chemical to Phenomenological Approaches* (R. Carbó, ed.), pp. 57-76. Kluwer Academic, Dordrecht, 1995.
- [39] P. G. Mezey, "Descriptors of Molecular Shape in 3D," in *From Chemical Topology to Three-Dimensional Geometry* (A. T. Balaban, ed.). Plenum, in press.
- [40] P. G. Mezey, "Functional Groups in Quantum Chemistry," in *Advances in Quantum Chemistry* (P.-O. Löwdin, ed.), Vol. 27, pp. 163-222. Academic Press, New York, 1996.

# 4

## **EEG Based Finger Induced Motor Imageries by Type-2 Fuzzy**

**Abstract-** This chapter presents a method for classification of individual fingers of one hand by motor imagery technique Electroencephalography (EEG). The EEG was recorded with 21 channel electrode array and the experiment was performed by eight healthy subjects. The classifiers used is Support vector machine and the feature taken is power spectral density and discrete wavelet transform. The Interval Type-2 Fuzzy Classifier has been used for discriminating individual fingers. The average decoding accuracy is 84% in an Intel Pentium Dual Core processor running Matlab R015b for each finger movement.

## 4.1 Introduction

The literature review of Brain computer interface has a vast research on discriminating individual fingers by the mostly used neuroimaging and non invasive method Electroencephalography(EEG). Decoding of brain activities that controls the devices which are assistive and other computer based applications is brain computer interface .

EEG[1-4] is a visual representation of electrical activities of the brain. It is a simple technology and relatively low cost than Magneto encephalography(MEG),Functional magneto resonance imaging(fMRI)[5] etc. Encouraged by some of the previous work, we aim at our research to classify method the single-finger movements from the EEG signal and analyze the different parts of motor cortex region for classification. EEG has a better temporal resolution. The selection of movement-related EEG is due to the natural to control anything with it .

We can use fuzzy logic in the classification of brain signals in the presence of noise and other brain activities . In classical Type-1 fuzzy set , the membership functions that are used cant capture the real experimental situation. So Type-2 fuzzy logic has been adapted which is capable to model the real world even in the presence of imperfections This paper proposed a novel approach to Interval Type-2 Fuzzy set(IT2FS)[6].The lower and upper firing strength of the inference are computed

Designation of Type-2 fuzzy classifier is done by type-2 fuzzy rules where the consequent[6] is the label of the class and antecedent is the propositions of fuzzy. Experiments undertaken confirms the accuracy of classification of the proposed type-2 fuzzy classifier design. Statistical test gives us a good performance of proposed one compared with others.

This paper includes six sections. Section II includes a system overview on the classification of individual fingers. Section III gives us the design of Type-2 fuzzy classifier. Section IV denotes the experiments and results. Statistical validation is evaluated in Section V. Finally comes the conclusion in Section VI.

## 4.2 System Overview

It gives us the overview of the system. There are 21 EEG electrodes used to record the brain signals. The e-LORETA software is used to obtain the activation regions of the brain for individual fingers. The elliptical band pass filter is chosen to acquire the brain signals. The artifact removal is done by Independent Component Analysis(ICA)[7].After removing the artifact feature extraction takes place. This leads to the classification of five fingers.

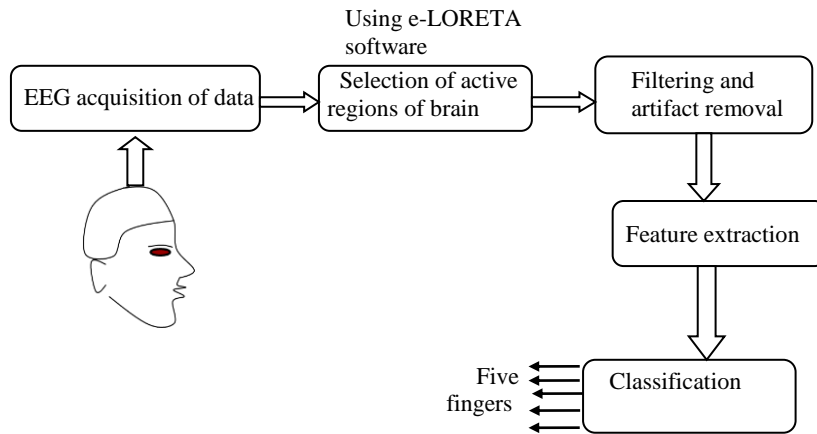


Fig.4.1. Block diagram of the system

### 4.3 Classifier Design

In the present motor imagery classification problem (for different fingers of a subject's hand), we model the fluctuation of the function (MF). Let  $x_1, x_2, \dots, x_n$  be  $n$  selected features acquired from hemodynamic features, of a particular day, by a Gaussian Membership the motor cortex region due to individual finger tapping motor imagery. The mean ( $m_{i,j}$ ) and variance ( $\sigma_{i,j}^2$ ) of the Gaussian type-1 MF are respectively the mean and the variance of the features obtained from a session for class . Each session comprises 10 trials. Thus we construct  $G(m_{i,j}, \sigma_{i,j}^2)$  for variation in feature over different sessions on different days. Now, to accommodate the effect of

these variations, we take the minimum and maximum of  $d$  days type-1 MF to construct the lower membership function (LMF) and upper membership function (UMF) respectively of an interval type-2 fuzzy sets (IT2FS). Thus for  $n$  features, we have  $n$  IT2FS given by  $[\underline{\mu}_{\tilde{A}_i}(x_i), \bar{\mu}_{\tilde{A}_i}(x_i)]$  for  $i= 1$  to  $n$ .

**4.3.1 Classifier Rule:** Let us consider, the classifier rule  $j$ , given by

*If  $x_1$  is  $\tilde{A}_{1,j}$  and  $x_2$  is  $\tilde{A}_{2,j}$  and... and  $x_n$  is  $\tilde{A}_{n,j}$ , then class =  $j$ .*

Suppose, we have  $n$  measurement points  $x_i = x'_i$  for  $i=1$  to  $n$  features. Now, we compute the Upper Firing Strength (UFS) and the Lower Firing Strength (LFS) of class  $j$  as:

$$UFS_j = \min(\bar{\mu}_{\tilde{A}_1}(x_1), \bar{\mu}_{\tilde{A}_2}(x_2), \dots, \bar{\mu}_{\tilde{A}_n}(x_n)) \quad (6)$$

$$LFS_j = \min(\underline{\mu}_{\tilde{A}_1}(x_1), \underline{\mu}_{\tilde{A}_2}(x_2), \dots, \underline{\mu}_{\tilde{A}_n}(x_n)) \quad (7)$$

We then compute the firing strength of class  $j$  by taking the weighted sum of  $UFS_j$  and  $LFS_j$  with respective weights  $w_j$  and  $(1-w_j)$ . So here

$$FS_j = w_j.UFS_j + (1-w_j).LFS_j \tag{8}$$

for any real number  $w_j$  in  $[0, 1]$ . A grid search algorithm [8] has been invoked ahead of classification for the selection of  $w_j$  with an aim to maximize the classification accuracy. Thus for five finger classes, we compute  $FS_j$  for  $j = 1$  to 5. If  $FS_j > FS_k \forall k$ , then the class= $j$  is inferred (Fig. 2).

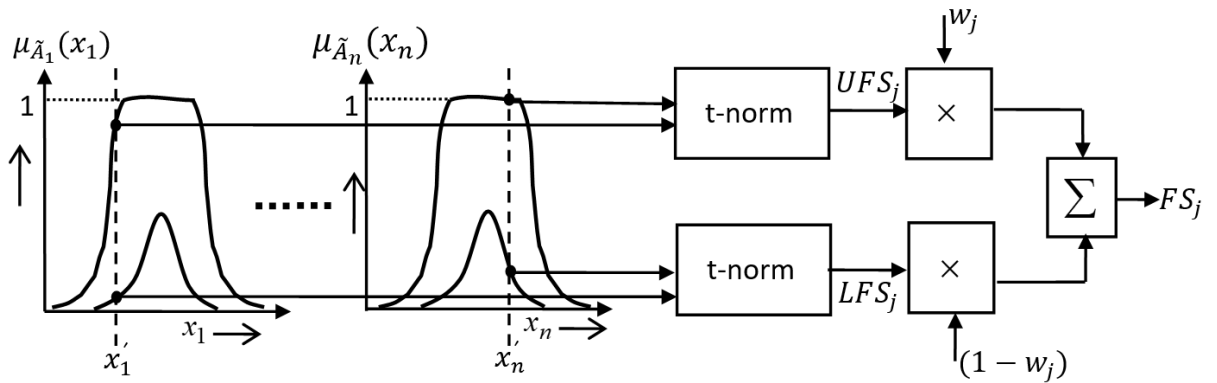


Fig .4.2. Architecture of Type-2 Fuzzy classifier

## 4.4 Experiments and Results

The section design the experiments to classify individual fingers.

### 4.4.1 Data Acquisition by EEG

The experiment is performed for 8 individuals present in the laboratory. They were instructed to perform repeated finger tapping activity according to the stimuli presented on the monitor. The experiment uses all the 21 electrodes namely temporal(T1,T2,T3,T4,T5,T6), prefrontal(Fp1,Fp2), frontal(F3,F4,F7,F8), occipital(O1,O2) and mainly the channels of the motor cortex region(C3, C4) gives more information to classify the fingers.

### 4.4.2 Source localization using e-LORETA software

The exact low resolution brain electromagnetic topographic analysis(e-LORETA)[9] software is used to determine the different activation regions of brain . It is used to reconstruct the cortical electrical activity with correct localization from the scalp EEG[10] data which was collected for 60s(=60000 millisecond) to get different results for the subjects.

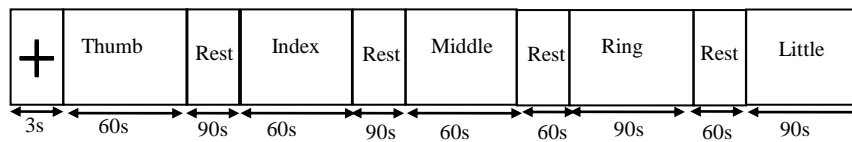


Fig. 4.3. Stimuli representation of individual fingers

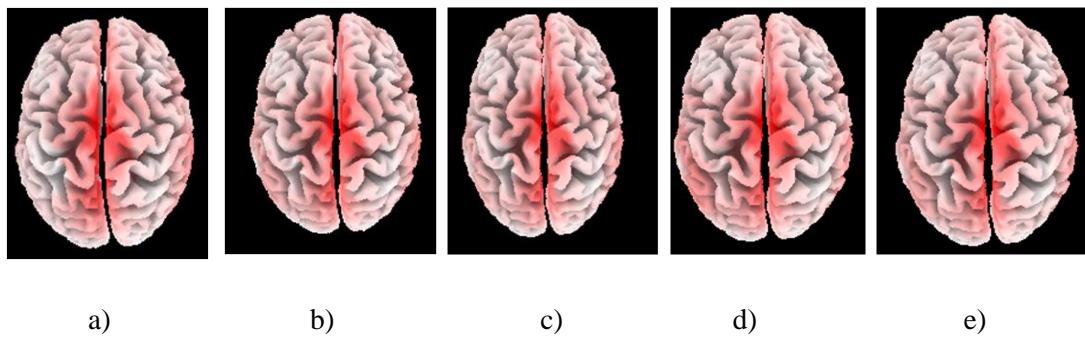
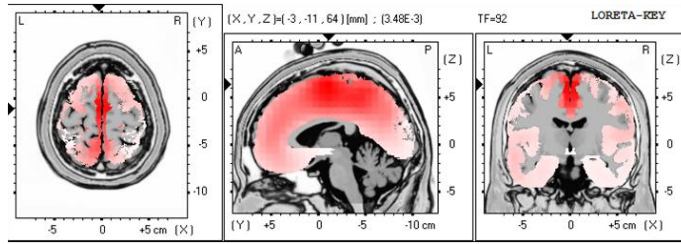
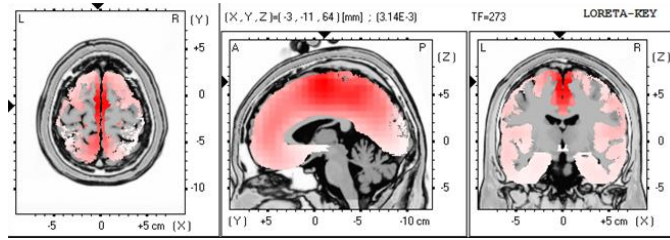


Fig 4.4. 3D view of Brain activation regions of a)Thumb b)Index c)Middle d)Ring e)Little

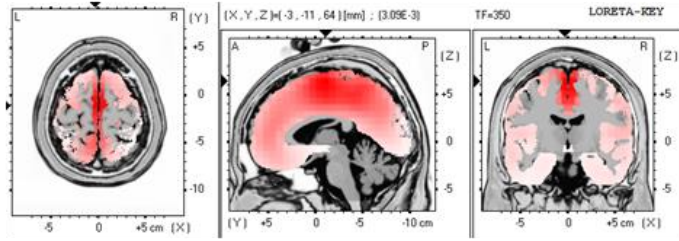




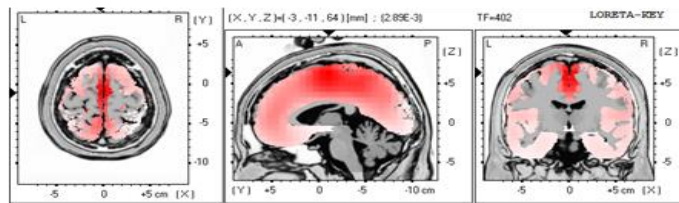
a)



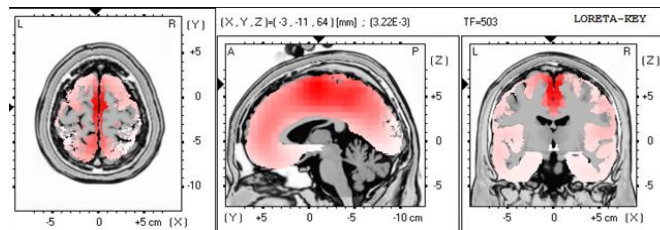
b)



c)



d)



e)

Fig 4.5 Brain activation region of a)Thumb b)Index c)Middle d)Ring e)Little

### 4.4.3 Filtering and Artifact Removal

Filtering is done by Infinite Impulse Response(IIR). Here Elliptic Pass bands of the filters are selected based on the association of the significant EEG bands (delta, theta, alpha, mu, beta and gamma) for a this task. Here Independent Component analysis is used for artifact removal.

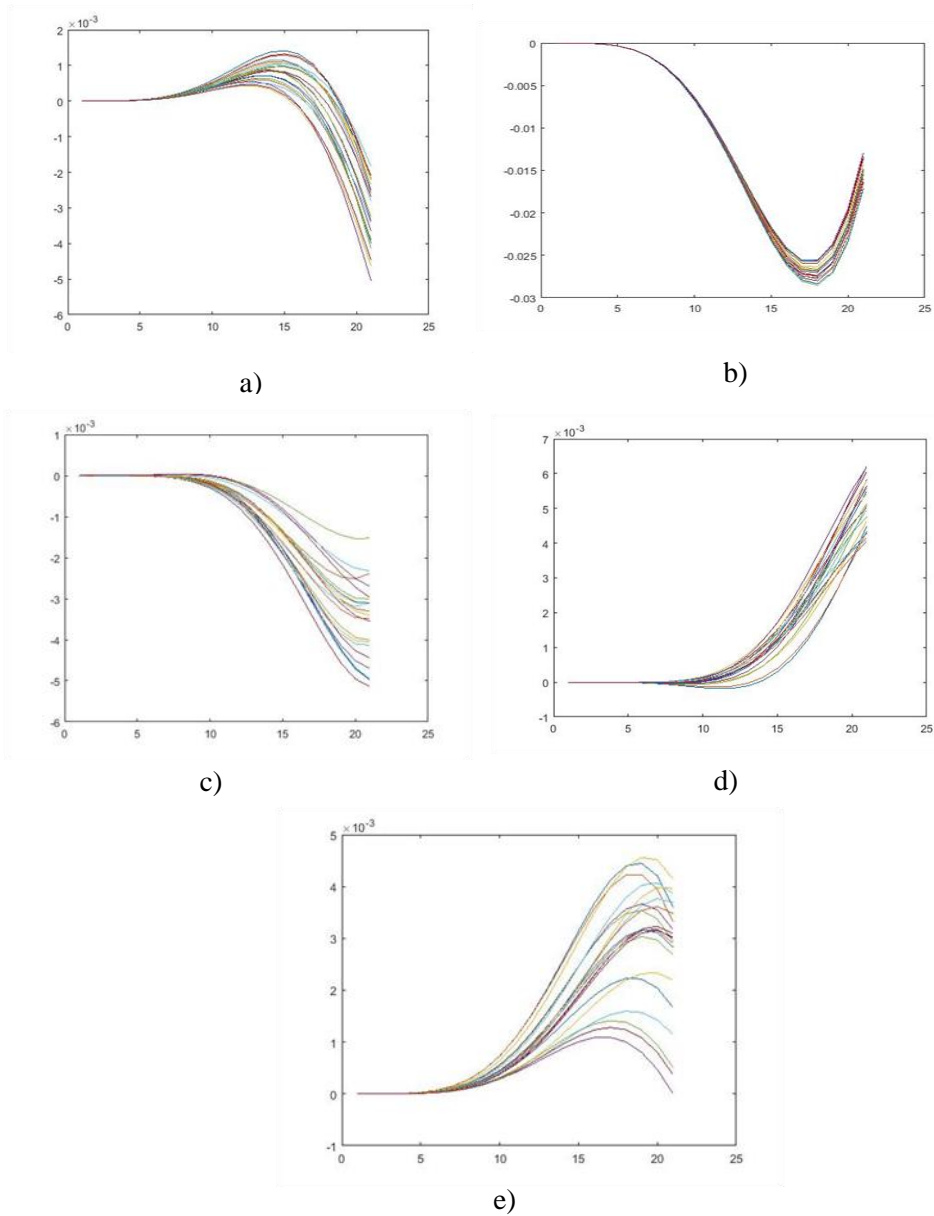


Fig 4.6 After Filtering and artifact removal a)Thumb b)Index c)Middle d)Ring e)Little

### 4.4.4 Feature Extraction

It extracts the EEG features i.e discrete wavelet transform[11] and power spectral density method[12]. Fig 3.6 denotes the PSD features from motor cortex region.

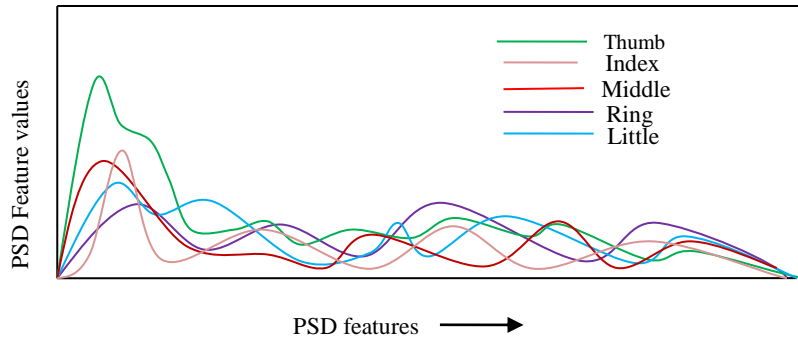


Fig 4.7.1 PSD feature extraction for five fingers from motor cortex region

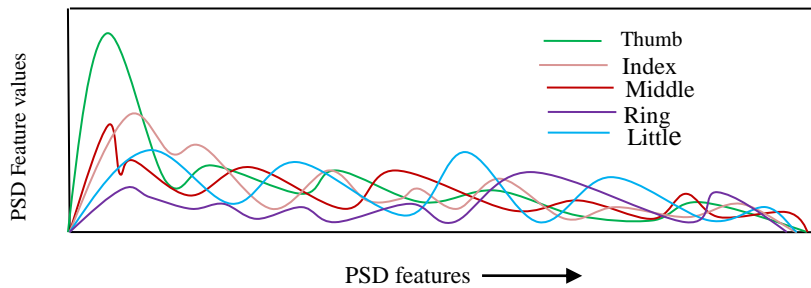


Fig 4.7.2 PSD feature extraction for five fingers from pre frontal region

## 4.5 Classifier Performance and Statistical Validation

This section deals with the experimental basis of performance analysis . Here the classification performance is divided into two phases: Training phase and Testing Phase

### 4.5.1.1 Training Phase

In this phase ten-fold cross validation is used . Nine folds are used for training data and another one is used for validation. Table 3.1 gives the performance of five fingers

**Table: 4.1** Classification accuracy for five fingers

Stimulus Type	Classification Accuracy(%)		
	Best	Average	Worst
Thumb	84.3	79.9	76.4
Index	83.6	79.1	75.7
Middle	83.1	78.2	73.6
Ring	81.9	76.8	69.8
Little	82.2	77.5	70.9

### 4.5.1.2 Testing Phase

A confusion matrix is created to determine the individual performance of the stimuli. Table 3.2 indicates that the classification of each class is high .

Table 4.2 Confusion matrix for classes

Actual class	Predict class				
	Thumb	Index	Middle	Ring	Little
Thumb	97.6	1.2	1.1	0.0	0.1
Index	1.3	96.7	1.4	0.1	0.5
Middle	0.2	1.6	96.1	1.5	0.6
Ring	0.1	1.9	2.3	94.8	0.9
Little	0.0	1.7	1.6	0.8	95.9

### 4.5.3 Relative performance analysis of the proposed classifier

To study the performance analysis, we compare the relative performance of the proposed classifier with traditional and existing classifiers. Here, we consider the following standard classifiers : linear support vector machine (LSVM) [13], polynomial kernel (KSVM-polynomial) [14], kernelized SVM using radial basis function (KSVM-RBF) [15], back propagation neural net (BPNN) [16], type-1 fuzzy system (Type-1 Fuzzy) and IT2FS. Table 2 provides the result of relative performance analysis of the proposed classifier outperforms the standard ones by quite a margin.

**Table 4.3** Relative performance analysis for Individual fingers (in %)

Classifiers	Thumb	Index	Middle	Ring	Little
LSVM	67.5	67.7	66.5	58.9	60.9
KSVM-polynomial kernel	73.8	70.9	72.6	69.7	72.7
KSVM-RBF kernel	76.5	74.4	74.8	71.6	72.9
BPNN	78.6	77.3	77.5	75.2	76.8
Type-1 Fuzzy	79.3	78.5	78.8	76.1	77.4
IT2FS	82.9	81.7	81.1	79.8	80.8
<b>Proposed Model</b>	<b>84.3</b>	<b>83.6</b>	<b>83.1</b>	<b>81.9</b>	<b>82.2</b>

### 4.5.4 Statistical Validation

. Table-3 presents the results of the statistical test by applying well-known Mc-Nemar's test [17]. Here, we consider two classifier algorithms  $X$  and  $Y$  where,  $X$  is the proposed IT2FS classifier algorithm and  $Y$  is the other standard classifiers listed in Table 3. Let us define two parameters  $n_{01}$  and  $n_{10}$ , where  $n_{01}$  be the number of classes misclassified by  $X$  but not by  $Y$ . On the other hand,  $n_{10}$  be the number of classes misclassified by  $Y$  but not by  $X$ . Then, we define,

$$z = \frac{(|n_{01} - n_{10}| - 1)^2}{n_{01} + n_{10}} \tag{9}$$

According to the  $\chi^2$  distribution table, we have  $\chi_{1,0.95}^2 = 3.84$  represents the value of Chi-square with probability 0.05 and the degree of freedom 1. The null hypothesis, representing that the two classifiers have identical performance with respect to the given classifier accuracy, is rejected as  $z$  exceeds  $\chi_{1,0.95}^2 = 3.84$ .

**Table 4.4** Statistical analysis with the reference algorithm: proposed IT2Fs classifier

Classifier algorithm used for comparison using desired features	Parameters used for McNemar’s test		z	Comments on acceptance/rejection of hypothesis
	$n_{01}$	$n_{10}$		
LSVM	31	97	33.01	Rejected
KSVM-polynomial kernel	17	67	28.58	Rejected
KSVM-RBF kernel	23	49	7.89	Rejected
BPNN	19	60	20.25	Rejected
Type-1 Fuzzy	23	49	8.68	Rejected
IT2FS	27	53	7.81	Rejected

## 4.6 Conclusion

This chapter gives the classification of finger motor imageries by EEG. A simple IT2FS induced fuzzy classifier is incorporated to classify the motor imageries of individual fingers of one hand to recognize the finger. Different parts of motor cortex region are activated for different fingers while tapping. Statistical (Mc Nemar’s) test undertaken also confirms the superiority of the proposed type-2 classifier.

## References

1. □ Quandt, F., Reichert, C., Hinrichs, H., Heinze, H. J., Knight, R. T., Rieger, J. W.: Single trial discrimination of individual finger movements on one hand: a combined MEG and EEG study. In: *NeuroImage*, 59(4), 3316-3324 (2012)
2. □ Paek, A. Y., Agashe, H., Contreras-Vidal, J. L.: Decoding repetitive finger movements with brain activity acquired via non-invasive electroencephalography. In: *Frontiers in neuroengineering*, 7(3) (2014)
3. □ Liao, K., Xiao, R., Gonzalez, J., Ding, L.: Decoding individual finger movements from one hand using human EEG signals. In: *PloS one*, 9(1), e85192 (2014).
4. □ Stankevich, L., Sonkin, K., Shemyakina, N., Nagornova, Z., Khomenko, J., Perets, D., Koval, A.: EEG pattern decoding of rhythmic individual finger imaginary movements of one hand. In: *Human Physiology*, 42(1), 32-42 (2016)
5. □ Liljeström, M., Hultén, A., Parkkonen, L., & Salmelin, R. Comparing MEG and fMRI views to naming actions and objects. *Human brain mapping*, 30(6), 1845-1856.(2009)
6. □ Mendel, J. M., John, R. I., Liu, F.: Interval type-2 fuzzy logic systems made simple. In: *IEEE Transactions on Fuzzy Systems*, 14(6), 808-821 (2006)
7. □ Kachenoura, A., Albera, L., Senhadji, L., & Comon, P. ICA: a potential tool for BCI systems. *IEEE Signal Processing Magazine*, 25(1), 57-68.(2007)
8. □ Hsu, C. W., Chang, C. C., Lin, C. J.: A practical guide to support vector classification. In: Department of Computer Science and Information Engineering, National Taiwan University, Taipei, Taiwan, <https://www.csie.ntu.edu.tw/~cjlin/papers/guide/guide.pdf>, (2003)
9. □ Laha, M., Konar, A., Rakshit, P., & Nagar, A. K.. EEG-Analysis for Classification of Touch-Induced Affection by Type-2 Fuzzy Sets. In 2018 IEEE Symposium Series on Computational Intelligence (SSCI) (pp. 491- 498) IEEE. (November 2018)
10. □ Chowdhury, M. M. H., & Khatun,: AImage compression using discrete wavelet transform. *International Journal of Computer Science Issues (IJCSI)*, 9(4), 327. . (2012).
11. □ Herman, P., Prasad, G., McGinnity, T. M., & Coyle, D.: Comparative analysis of spectral approaches to feature extraction for EEG-based motor imagery classification. *IEEE Transactions on Neural Systems and Rehabilitation Engineering*, 16(4), 317-326. (2008).
12. □ Pan, F., Wang, B., Hu, X., Perrizo, W.: Comprehensive vertical sample-based KNN/LSVM classification for gene expression analysis. In: *Journal of Biomedical Informatics*, 37(4), 240-248 (2004)
13. □ Kejia, X., Zhiying, T., Bin, C.: Reweighting Recognition Using Modified Kernel Principal Component Analysis via Manifold Learning. In: *Advanced Technology in Teaching-Proceedings of the 2009 3rd International Conference on Teaching and Computational Science (WTCS 2009)*, 609-617, Springer, Berlin, Heidelberg (2012)
14. □ Ravale, U., Marathe, N., Padiya, P.: Feature selection based hybrid anomaly intrusion detection system using K means and RBF kernel function. In: *Procedia Computer Science*, 45, 428-435 (2015)
15. □ Dao, V. N., Vemuri, V. R.: A performance comparison of different back propagation neural networks methods in computer network intrusion detection. In: *Differential Equations and Dynamical Systems*, 10, 201-214 (2002)
16. □ Sun, X., Yang, Z. : Generalized McNemars test for homogeneity of the marginal distributions. In: *SAS Global Forum*, 382, 1-10 ( March, 2008)

# 5

## **Finger Induced Motor Imageries from Hemodynamic Response using Type-2 Fuzzy sets**

**Abstract-** Although there exists significant research results on left/right hand motor imageries, there is a scarcity of research on the classification of individual finger movements by motor imagery techniques. This paper provides a solution to this open problem by proposing an advanced classifier to classify the finger motor imageries corresponding to the motor intentions at individual fingers of the right hand with the help of functional near infrared spectroscopy (fNIRS) based hemodynamic response of the human brain. Experimental results obtained confirm that the proposed hemodynamic response based classification outperforms the reported results of electroencephalography (EEG) based classification in terms of classification accuracy. Statistical tests included confirm the efficacy of the proposed technique over its competitors.



## 5.1 Introduction

Humans like most other mammals use their motor cortex region to control voluntary movements of their body parts. Several interesting research works, concerning motor movement control, have been published in the past [1–6]. Most of the existing research is conducted using left and/or right hand motor imageries, obtained from EEG devices [2–6]. This paper, however, has a different motivation. It aims at classifying motor intentions of individual fingers from the hemodynamic response, captured by a full-brain fNIRS device. To the best of the authors knowledge, this is the first work of its kind, where fNIRS based hemodynamic response is used for classification of individual finger motor imagery. Infrared imagery is preferred over EEG for its good spatial resolution [7] like functional Magnetic Resonance Imaging (fMRI) devices. The fNIRS devices have an advantage of having relatively low price while at the same time give acceptable performance. This prompted us to use fNIRS device for our motor imagery classification.

Mental translation of motor imagination to real execution is possible with the advent of left/right hand motor imagery as in [6], where left/right hand motor imageries were used for on-off type motor movement control, where the decoded left hand imagery was used to make a device on and the right hand imagery to make it off. However, for complex branching tasks, complex coding techniques are required for left/right hand motor imagery [8]. For example, a 3-bit coding can produce 8 patterns with L (for left-hand) and R (for right-hand) motor imageries, where 3 successive mental imaginations for the left/right hand movements are required to generate a 3-bit code word like L-R-L, L-L-L, R-L-L and the like. Such coding requires additional decoding to get back the intended motor action by the subject. Both encoding and decoding operations can be avoided, in case the finger motor imageries could be decoded correctly by a suitable classifier. In

fact, 10 different motor actions, say, for setting motion of a robot in 10 different directions at  $36^\circ$  intervals, can be realized with a single-bit binary classifier for each finger motor imagery. Again for branching tasks, left/right hand imagery can be used to steer an automated guided vehicle (AGV) clockwise or counterclockwise and then to select its steering angle. Such AGVs can be driven by the motor imaginations of an amputee.

The fNIRS device measures the change in oxygenated and deoxygenated blood in response to a cognitive task undertaken by the brain [9]. It is observed that the difference in oxygenated and deoxygenated blood response to motor-imagery task is prominent, and thus is used as the basis for motor classification. To make the performance robust, the duration of fNIRS acquisition is divided into 3 time-slots, and the mean, variance, skewness, kurtosis, average slope and the average energy of the sample points within each slot are used as the static features. Besides static features, dynamic features, representing changes in the above parameters over the 3-time-slots are also considered. Further, because of the presence of physiological noise, like eye blinking, heart-beat, respiration, blood pressure fluctuation and mere waves, the fNIRS features may suffer from imprecision.

Fuzzy logic has shown promising results in classification of brain signals in presence of noise in the acquired brain responses due to parallel thoughts and other concurrent undesirable brain activities. Membership functions used in classical (type-1) fuzzy sets are constructed from single source, and thus can hardly capture the real experimental situation. Type-2 fuzzy logic, on the other hand, has added advantage of integratings opinion of several sources, and thus is capable to model the real world, even in presence of noise/imperfections. This inspired us to design the classifier using type-2 fuzzy sets.

Two well-known varieties of type-2 fuzzy sets are popularly known in the literature. They are interval type-2 fuzzy set (IT2FS) [10] and general type-2 fuzzy sets (GT2FS) [11]. Although GT2FS has better potential in capturing the real world uncertainty, it is hardly used in practice for its high computational overhead. In this paper, the authors employed IT2FS to undertake motor imagery classification from noisy fNIRs signals as in [12].

The type-2 classifier is designed using type-2 fuzzy rules, where the antecedent of each rule includes fuzzy propositions, representing linguistic variables with their interval type-2 membership functions (IT2MFs) and the consequent includes a class label [10]. For a given set of measurements of the linguistic variables used in the rule, the upper and lower firing strength of the inference are computed. A weighted sum of the upper and lower firing strengths [13] is finally used as the effective firing strength. Thus for a given set of measurements all the rules are fired, and the rule having the highest firing strength is identified. In case the rule with highest firing strength is rule  $j$ , then class  $j$  indicates the motor imagery of the  $j^{\text{th}}$  finger.

As the weights of the upper and lower firing strength have impact on the firing strength computation, we need to optimally select the weights ahead of classification. This is done by preparing a table of training instances with class labels. Experiments are carried out to search the proper choice of the weights to maximize the classification accuracy. In this paper a simple grid search algorithm [14] is computed for the optimal selection of weights of the lower and upper firing strengths for each rule. Experiments undertaken confirm that the classification accuracy of the proposed type-2 fuzzy classifiers outperforms traditional classifiers. Statistical test undertaken reveals the superior performance of the proposed technique over others.

The paper includes six sections. In section 2, we provide a general overview of the proposed system. In Section 3, we introduce a novel scheme for type-2 fuzzy classifier design. Section 4 provides experimental details and their results. The performance analysis and statistical validation is included in Section 5. The conclusions are summarized in Section 6.

## 5.2 Principles and Methodology

The finger based motor imagery classification is performed in five main steps: data acquisition and normalization of the fNIRS signals, pre-processing and artifact removal, feature extraction, feature selection, and classification. Fig. 1 outlines the basic scheme of finger tapping based motor imagery classification.

The following principle is adopted to normalize the acquired hemodynamic response. Let  $C_{HbO_\alpha}(t)$  and  $C_{HbR_\alpha}(t)$ , respectively be the oxygenated and the de-oxygenated blood response of the  $\alpha$ -th channel, in the motor-cortex for motor imagery classification. The following two parameters are evaluated to normalize  $C_{HbO_\alpha}(t)$  and  $C_{HbR_\alpha}(t)$  respectively, at the given  $\alpha$ th channel:

$$\max C_{HbO} = \max_t (C_{HbO_\alpha}(t) : t_0 \leq t \leq T, \forall \alpha) \quad (1)$$

$$\min C_{HbR} = \min_t (C_{HbR_\alpha}(t) : t_0 \leq t \leq T, \forall \alpha) \quad (2)$$

where  $t_0$  and  $T$  respectively denote the beginning and the end time of an experimental trial for a given stimulus on a selected subject.

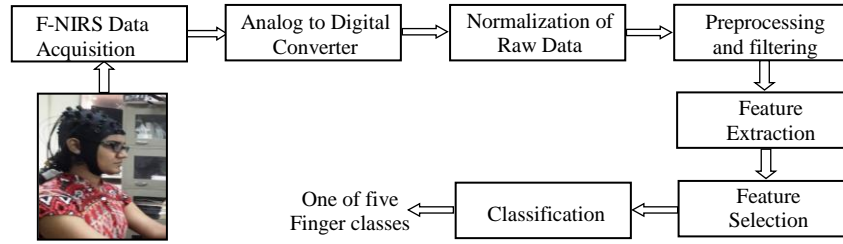


Fig.5.1 System overview of the finger classification

The normalized value of the difference signal

$$d_{\alpha}(t) = C_{HbO_{\alpha}}(t) - C_{HbR_{\alpha}}(t), \quad (3)$$

$$\hat{d}_{\alpha}(t) = \frac{(C_{HbO_{\alpha}}(t) - C_{HbR_{\alpha}}(t))}{\max C_{HbO}(t) - \min C_{HbR}(t)} \quad (4)$$

is obtained as

The sampling rate of the fNIRs device is 7.8 samples/sec. In the training phase, each trial contains  $15 \times 7.8 = 117$  samples. The 15 seconds duration is divided into 3 time-windows, each window includes  $117 \div 3 = 39$  samples. Next, the normalized difference signal  $\hat{d}_{\alpha}(t)$  for  $\alpha = 1$  to  $M$  channels is passed through a Elliptic Band Pass Filter of order 10. with the cut off frequencies at 0.1 and 5 Hz, to remove various forms of physiological artifacts [15]. The selection of elliptic band pass filter is induced by its sharp roll off around the cut-off frequency. Next, we compute the static features which include mean, standard deviation, skewness , kurtosis, signal slope and average energy of  $\hat{d}_{\alpha}(kt)$ , at  $t = kT, k = 0,1,2, \dots$ . We also compute the dynamic features obtained by taking the difference of static features in a trial. Let  $\hat{d}_{i,\alpha}(kt)$  denote the  $i^{th}$  static feature of the  $\alpha^{th}$  channel for  $i = 1$  to  $n$  and  $\alpha = 1$  to  $M$ . So the  $i^{th}$  dynamic feature from the  $\alpha^{th}$  channel is obtained by

$$\Delta \hat{d}_{i,\alpha}(kt) = \hat{d}_{i,\alpha}(kt) - \hat{d}_{i,\alpha}((k-1)T) \quad (5)$$

In the present application, we have  $6 \times 3 = 18$  static features and  $6 \times 2 = 12$  dynamic features.

Consequently, we have  $18 + 12 = 30$  features for each channel, thereby providing

$M \times n = 20 \times 30 = 600$  features per individual subject. The product  $M \times n$  being large enough, we adopt Differential Evolutionary (DE) algorithm [16] based feature selection method to reduce 600 features into 150 optimal features.

After feature selection is over, the fNIRS features are fed to a classifier to classify the motor imagery task into one of the five finger classes. The classification undergoes both training and test phases. In the training phase, the classifier parameters/weights are adapted. In the test phase, the weights/classifier parameters are known. Only, the input fNIRS features are submitted to the classifier and the classifier needs to produce the right class for the given set of input features. Although any traditional classifier could serve the purpose, a type-2 fuzzy logic induced classifier is employed here to eliminate the influence of noise in the acquired fNIRS signals in the classification process. As mentioned earlier some noise may creep into fNIRS signals because of the parallel engagement of brain lobe due to side thoughts, eye-blinking and other artifacts. Type-2 fuzzy sets have proved itself successful to classify noisy features into classes with high classification accuracy. Details of type-2 fuzzy classifier are explained next.

### 5.3 Classifier Design

The classifier design refers to chapter 4.

## 5.4 Experiments and Results

This section includes three following experiments to obtain the main results of the finger-induced

motor imagery classification. Experiment 1 is concerned with the automatic feature extraction to identify the correct fingers. Experiment 2 provides the selection of hemodynamic features using differential evolutionary algorithm. In experiment 3 we analyse the topographic map of five fingers for each subjects.

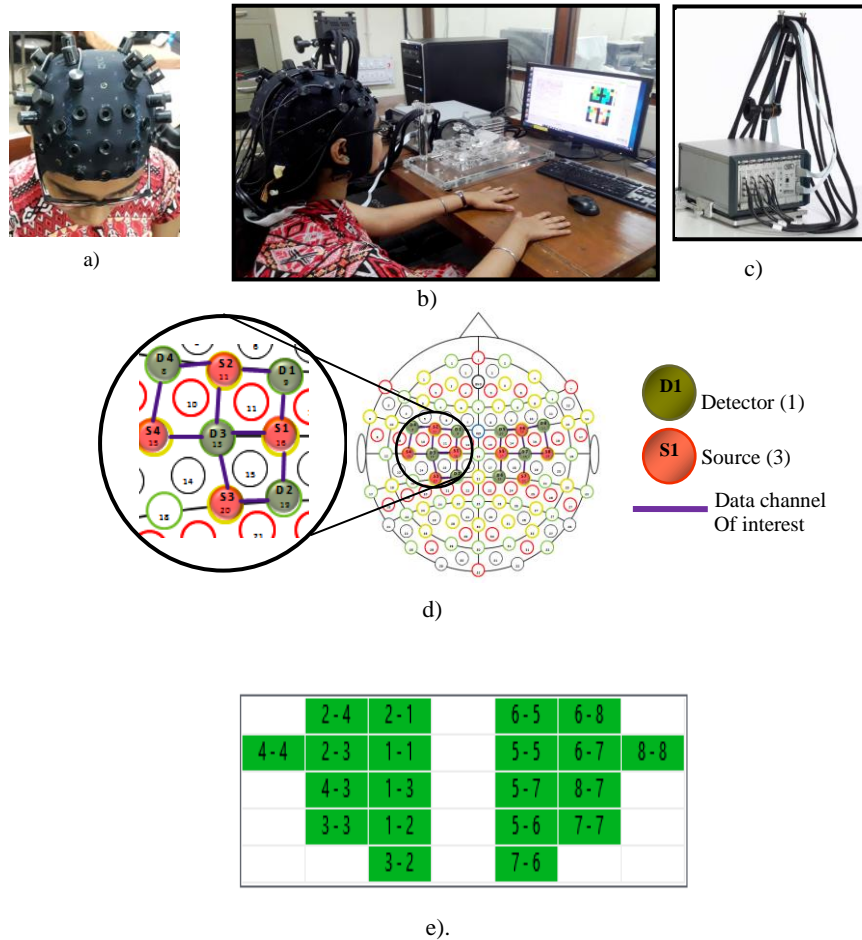


Fig 5.2 a) f-NIRs Cap b) Experimental Set-up c) f-NIRs device d) Source-detector connection of motor-cortex\_8x8 montage e) Channel set-up for motor-cortex montage.

### 5.4.1 f-NIRs data acquisition and experimental framework

The experiment is performed in Artificial Intelligence Laboratory of Jadavpur University, Kolkata, India. Experiments were performed in a well insulated room where the subjects were seated comfortably in an armchair. They were instructed to perform repeated finger tapping activity according to the stimuli presented on the monitor. The fNIRS signals were recorded from NIRX Nirxcout NIRS imager, manufactured by NIRx Medical Technologies LLC, using 8 infrared (IR) sources and 8 IR detectors, placed over the scalp of the subjects according to the international 10-10 system and in order to capture the hemodynamic response of the brain, observations made at two different frequencies (760 nm & 850 nm) and a sampling rate of 7.892 Hz (Fig. 3(a,b,c)). The source-detector arrangement on the head to the topographic layout is shown in Fig. 3(d). The neighboring source-detector combination forms a data channel. Here 8 sources and 8 detectors forms  $8 \times 8 = 64$  channels, of which 20 channels are selected followed by nearest neighboring source-detector combinations according to 10-10 placement system. Fig. 3(e) identifies the selected combination of channels. Here, for example, the channel 3 represents the IR pathway from source 2 to detector 3, and is positioned at the top left corner in the topographic layout. Ten healthy volunteers participated in the said experiment which included six men and four women in the age-group of 22-30 years.

### 5.4.2 Stimuli Presentation for Online Classification

Each subject is advised to tap one of the five fingers (Thumb, Index, Middle, Ring or Little) for 15 s duration as per the visual cue. In order to eliminate the residual effect of one finger tapping to the next, a 10 s time-delay is introduced between each pair of successive finger-tapping. The experiment includes 10 sessions, where each session includes 10 trials. Consequently for 10



healthy subjects we have  $10 \times (10 \text{ session/stimuli}) \times (10 \text{ trials/session}) \times (5 \text{ stimulus/trial}) = 5000$  training instances are generated to classify five fingers. Fig. 4 provides a sample structure of the stimulus presented in the said experiment for a single trial.

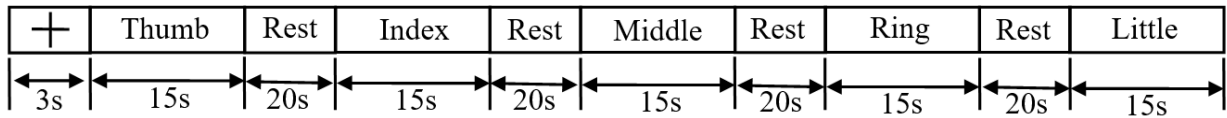


Fig.5.3. Sample single trial visual-cue for finger induced motor imagery stimuli

### 5.4.3 Experiment 1: Extraction Of Hemodynamic features to discriminate Individual fingers

The motivation of the experiment is to extract the f-NIRs features for five different fingers tapping induced motor imagery from the hemodynamic response of the brain. Fig. 5 represents the feature level discrimination of the mean HbO concentration of the five fingers to classify the five classes. Eight optimal features out of 600 are selected from the feature value plot (Fig. 5) for five classes. It is evident from the plot that the feature f81 (mean HbO concentration of channel 4), f123 (mean HbO concentration of channel 6), f158 (mean HbO concentration of channel 9), f262 (mean HbO concentration of channel 7), f322 (mean HbO concentration of channel 19), f358 (mean HbO concentration of channel 15), f428 (mean HbO concentration of channel 19), f525 (mean HbO concentration of channel 19) offer maximal intra-class separation.

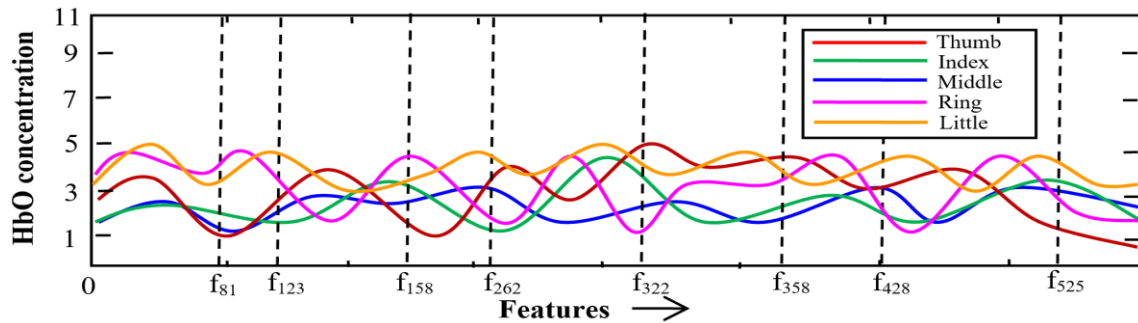


Fig.5.4. Feature level discrimination between mean HBO concentration for five fingers

#### 5.4.4 Experiment 2: Selection of the Discriminating Hemodynamic features using DE

The motivation of this experiment is to select the most significant features from a large dimensional feature sets, (here, 600) by Differential Evolutionary algorithm. The feature selection algorithm provides 150 optimal features. Out of 150 optimal features the best 8 features are plotted in Fig. 5. The result of the proposed evolutionary algorithm based feature selection is compared with the other traditional PCA technique in Table I. It is evident from table-I that the proposed feature selection process gives better classification accuracy of the classifier.

#### 5.4.5 Experiment 3: Topographic Map Analysis for individual fingers

This experiment provides that the corresponding changes in the topographic maps for individual fingers. Different regions are activated for the individual finger-imageries in Fig. 6, as indicated. The primary motor cortex of the left hemisphere and pre motor cortex of the right hemisphere are mainly activated for the index finger; the primary motor cortex of the left and right hemisphere are activated for the ring finger; the supplementary motor cortex of the left and right

hemisphere are activated for the thumb; the supplementary motor cortex of the left hemisphere and the primary motor cortex of the right hemisphere are activated for the middle finger; the pre motor cortex of the left hemisphere and the primary motor cortex of the right hemisphere are activated for the little finger.

TABLE 5.1. A Comparison between PCA and proposed feature selection technique with the proposed IT2FS classifier

Stimulus	Classification Accuracy (standard deviation)	
	PCA+ Proposed classifier algorithm	DE+ Proposed classifier algorithm
Thumb	89.6 (0.0172)	<b>92.8 (0.0112)</b>
Index	85.7 (0.0234)	<b>89.7 (0.0155)</b>
Middle	86.5 (0.0065)	<b>89.2 (0.0042)</b>
Ring	82.1 (0.0312)	<b>85.3 (0.0212)</b>
Little	84.9 (0.0294)	<b>88.7 (0.0197)</b>

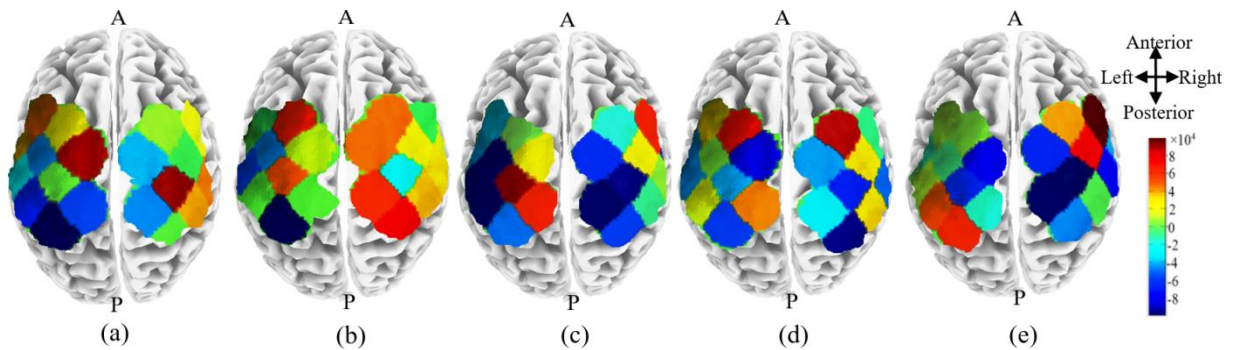


Fig 5.5 Brain activation region for (a)Thumb (b)Index (c)Middle (a)Ring (a)Little during one of the experimental trial

## 5.5 Classifier Performance and Statistical Validation

This section deals with the experimental basis of performance analysis of the proposed Type-2 fuzzy set induced reasoning techniques with the traditional and existing ones.

### 5.5.1 Relative performance analysis of the proposed classifier

To study the performance analysis, we compare the relative performance of the proposed classifier with traditional and existing classifiers. Here, we consider the following standard classifiers : linear support vector machine (LSVM) [17], polynomial kernel (KSVM-polynomial) [18], kernelized SVM using radial basis function (KSVM-RBF) [19], back propagation neural net (BPNN) [20], type-1 fuzzy system (Type-1 Fuzzy) and IT2FS. Table 2 provides the result of relative performance analysis of the proposed classifier outperforms the standard ones by quite a margin. It is also apparent from the Table-2 that the run time complexity of the proposed classifier takes 42.9 milliseconds, which is comparably less than the other existing classifiers

**Table 5.2.** Relative performance analysis for Individual fingers (in %)

Classifiers	Thumb	Index	Middle	Ring	Little	Run-time complexity
LSVM	69.1	69.3	68.7	60.2	62.3	53.0 ms
KSVM-polynomial kernel	75.1	72.6	74.2	71.9	74.6	55.1 ms
KSVM-RBF kernel	78.2	76.1	76.9	73.3	74.9	60.2 ms
BPNN	85.9	83.2	83.8	80.6	82.9	67.3 ms
Type-1 Fuzzy	88.6	84.9	84.4	82.8	85.2	49.8 ms
IT2FS	89.7	85.2	86.1	83.7	84.4	44.4 ms
<b>Proposed Model</b>	<b>92.8</b>	<b>89.7</b>	<b>89.2</b>	<b>85.3</b>	<b>88.7</b>	<b>42.9 ms</b>

### 5.5.2 Statistical Validation

Table-3 presents the results of the statistical test by applying well-known Mc-Nemar's test [21]. Here, we consider two classifier algorithms  $X$  and  $Y$  where,  $X$  is the proposed IT2FS classifier algorithm and  $Y$  is the other standard classifiers listed in Table 3. Let us define two parameters  $n_{01}$  and  $n_{10}$ , where  $n_{01}$  be the number of classes misclassified by  $X$  but not by  $Y$ . On the other hand,  $n_{10}$  be the number of classes misclassified by  $Y$  but not by  $X$ . Then, we define,

$$z = \frac{(|n_{01} - n_{10}| - 1)^2}{n_{01} + n_{10}} \tag{6}$$

According to the  $\chi^2$  distribution table, we have  $\chi_{1,0.95}^2 = 3.84$  represents the value of Chi-square with probability 0.05 and the degree of freedom 1. The null hypothesis, representing that the two classifiers have identical performance with respect to the given classifier accuracy, is rejected as  $z$  exceeds  $\chi_{1,0.95}^2 = 3.84$ .

**Table 5.3.** Statistical analysis with the reference algorithm: proposed IT2Fs classifier

Classifier algorithm used for comparison using desired features	Parameters used for McNemar's test		z	Comments on acceptance/rejection of hypothesis
	$n_{01}$	$n_{10}$		
LSVM	31	97	33.01	Rejected
KSVM-polynomial kernel	17	67	28.58	Rejected
KSVM-RBF kernel	23	49	7.89	Rejected
BPNN	19	60	20.25	Rejected
Type-1 Fuzzy	23	49	8.68	Rejected
IT2FS	27	53	7.81	Rejected

### 5.5.3 Performance Analysis with the Previous Work

Table 4 provides the performance analysis of the proposed technique with the existing work [4]. In [4], the authors have performed the experiments using EEG signals. It is evident from Table 4 that the classification accuracy of the proposed algorithm from the hemodynamic response acquired from the fNIRS device has the superior performance than the existing work.

**Table 5.4.** A Comparison between the classification accuracy measures of the proposed method and the existing work

	Proposed Algorithm	Algorithm proposed in [4]
Accuracy Measure	<b>85.3 - 92.8 %</b>	71.43 - 82.41 %

## 5.6 Conclusion

Classification of finger motor imageries is an open problem till date. This paper introduces an interesting approach to solve this open problem by employing a fNIRS device to measure the hemodynamic information from active brain regions. A simple IT2FS induced fuzzy classifier is incorporated to classify the motor imageries of individual fingers of one hand to recognize the finger. Experiments undertaken confirm the superior performance of the proposed fuzzy classifier with respect to the state-of-the-art techniques. Statistical (Mc Nemar's) test undertaken also confirms the superiority of the proposed type-2 classifier.

## References

1. Gundelakh, F., Stankevich, L., Sonkin, K.: Mobile robot control based on noninvasive brain-computer interface using hierarchical classifier of imagined motor commands. In: MATEC Web of Conferences, 161, 03003. EDP Sciences (2018)
2. Quandt, F., Reichert, C., Hinrichs, H., Heinze, H. J., Knight, R. T., Rieger, J. W.: Single trial discrimination of individual finger movements on one hand: a combined MEG and EEG study. In: NeuroImage, 59(4), 3316-3324 (2012)
3. Paek, A. Y., Agashe, H., Contreras-Vidal, J. L.: Decoding repetitive finger movements with brain activity acquired via non-invasive electroencephalography. In: Frontiers in neuroengineering, 7(3) (2014)
4. Liao, K., Xiao, R., Gonzalez, J., Ding, L.: Decoding individual finger movements from one hand using human EEG signals. In: PloS one, 9(1), e85192 (2014).
5. Stankevich, L., Sonkin, K., Shemyakina, N., Nagornova, Z., Khomenko, J., Perets, D., Koval, A.: EEG pattern decoding of rhythmic individual finger imaginary movements of one hand. In: Human Physiology, 42(1), 32-42 (2016)
6. Bhattacharyya, S., Khasnobish, A., Konar, A., Tibarewala, D. N., Nagar, A. K.: Performance analysis of left/right hand movement classification from EEG signal by intelligent algorithms. In: 2011 IEEE Symposium on Computational Intelligence, Cognitive Algorithms, Mind, and Brain (CCMB), Paris. IEEE (April, 2011)
7. Yin, X., Xu, B., Jiang, C., Fu, Y., Wang, Z., Li, H., Shi, G.: A hybrid BCI based on EEG & fNIRS signals improves performance of decoding motor imagery of both force & speed of hand clenching. In: Journal of Neural Engineering, 12(3), (2015)
8. Khasnobish, A., Jati, A., Singh, G., Bhattacharyya, S., Konar, A., Tibarewala, D.N., Nagar, A. K.: Object-shape recognition from tactile images using a feed-forward neural network. In: The 2012 International Joint Conference on Neural Networks (IJCNN), Brisbane, Queensland. IEEE (June, 2012)
9. De, A., Konar, A., Samanta, A., Biswas, S., Ralescu, A. L., Nagar, A. K.: Cognitive load classification in learning tasks from hemodynamic responses using type-2 fuzzy sets. In: 2017 IEEE International Conference on Fuzzy Systems (FUZZ-IEEE), Naples. IEEE (July, 2017)
10. Mendel, J. M., John, R. I., Liu, F.: Interval type-2 fuzzy logic systems made simple. In: IEEE Transactions on Fuzzy Systems, 14(6), 808-821 (2006)
11. Mendel, J. M.: General type-2 fuzzy logic systems made simple: a tutorial. In: IEEE Transactions on Fuzzy Systems, 22(5), 1162-1182 (2014)
12. Ghosh, L., Konar, A., Nagar, A.K.: Hemodynamic Analysis for Cognitive Load Assessment and Classification in Motor Learning Tasks using Type-2 Fuzzy Sets. In: IEEE Transactions on Emerging Topics in Computational Intelligence (E.A.)
13. Saha, A., Konar, A., Nagar, A. K.: EEG analysis for cognitive failure detection in driving using type-2 fuzzy classifiers. In: IEEE Transactions on Emerging Topics in Computational Intelligence, 1(6), 437-453 (2017)
14. Hsu, C. W., Chang, C. C., Lin, C. J.: A practical guide to support vector classification. In: Department of Computer Science and Information Engineering, National Taiwan University, Taipei, Taiwan, <https://www.csie.ntu.edu.tw/~cjlin/papers/guide/guide.pdf>, (2003)

15. Naseer, N., Hong, K. S.: fNIRS-based brain-computer interfaces: A review. In: *Frontiers in human neuroscience*, 9(3) (2015)
16. Basu, D., Bhattacharyya, S., Sardar, D., Konar, A., Tibarewala, D. N., Nagar, A.K.: A differential evolution based adaptive neural Type-2 Fuzzy inference system for classification of motor imagery EEG signals. In: *2014 IEEE International Conference on Fuzzy Systems (FUZZ-IEEE)*. IEEE (July, 2014)
17. Pan, F., Wang, B., Hu, X., Perrizo, W.: Comprehensive vertical sample-based KNN/LSVM classification for gene expression analysis. In: *Journal of Biomedical Informatics*, 37(4), 240-248 (2004)
18. Keja, X., Zhiying, T., Bin, C.: Reweighting Recognition Using Modified Kernel Principal Component Analysis via Manifold Learning. In: *Advanced Technology in Teaching-Proceedings of the 2009 3rd International Conference on Teaching and Computational Science (WTCS 2009)*, 609-617, Springer, Berlin, Heidelberg (2012)
19. Ravale, U., Marathe, N., Padiya, P.: Feature selection based hybrid anomaly intrusion detection system using K means and RBF kernel function. In: *Procedia Computer Science*, 45, 428-435 (2015)
20. Dao, V. N., Vemuri, V. R.: A performance comparison of different back propagation neural networks methods in computer network intrusion detection. In: *Differential Equations and Dynamical Systems*, 10, 201-214 (2002)
21. Sun, X., Yang, Z. : Generalized McNemars test for homogeneity of the marginal distributions. In: *SAS Global Forum*, 382, 1-10 ( March, 2008)



# 6

## VR based Cognitive Load Test

### Abstract

BCI based cognitive load assessment has been a topic of significant research for quite some time, especially while considering the driving scenario. However till date very few research documents have considered its evaluation in a VR environment and none providing a qualitative or a quantitative analysis between the two. Through this chapter we would try to provide a quantitative analysis of EEG-based cognitive load test while driving in a VR environment compared to that in the non-VR environment.

### 6.1 Introduction

Evaluation of cognitive load test using EEG has been a popular research study.

Cognitive failure while driving due to lapse of visual alertness, cognitive planning, and motor execution was studied in [1]. Recurrent Neural Networks

(RNN) classifiers on the basis of Lyapunov energy surface were used for the processing of EEG signals. The work was further extended in [2], employing a novel two-stage motor intention classifier. A differential Evolution (DE)-induced fuzzy neural classifier was used for the decoding and classification of motor imagery potentials while driving in [3]. As an improvement, authors in [4], proposed a novel General-Type-2-Fuzzy (GT2FS) and Interval-Type-2-Fuzzy (IT2FS) sets for cognitive load test while driving and was shown to outperform the existing classifier. This work considered event-related desynchronization (ERD) and event-related synchronization (ERS) stimuli responses, and was extended in [5] using P-300 and N-400 stimuli responses. Different from the existing work, author in [6], performed the analysis of cognitive load test while driving using fNIRS for better spatial response of the stimuli.

In 2002, authors in [7] provided a glimpse of possible VR applications into different contexts of user-interface. Later, the VIRART team from University of Nottingham, presented in [8] and [9]. In [10], a detailed study on a driver's working memory load assessment with the help of fNIRS was performed using a very realistic VR driving simulator setup at German Aerospace Centre. Similarly in [11], a study on multitasking while driving in a with participants of different age groups. However, both the above research considered either multiple displays or a very large screen, which is not very cost-effective and also a fixed simulator, for representing a VR environment. Contrary to this, authors in [12] considered a head-mounted display (HMD)-based VR and studied the efficiency of the HMD-VR over traditional fixed simulations, based on a fixed set of questionnaires. Since subjective questionnaires can't be

considered as optimal human-machine interface performance indicator [13], we tried to evaluate the cognitive load test while HMD-VR based driving simulations, using EEG responses to different responses during simulation.

As, it can be observed that researches now prefer evaluation of cognitive load test in virtual-reality environments as compared to traditional simulation environments. The reasons could obviously be linked to the better interactive capability of VR which results in a more natural response. However, so far to the best of authors knowledge, till date no study has been done to compare and evaluate the performance of the two techniques qualitatively or quantitatively. Hence based on different statistical measures, this chapter tries to provide a comparative analysis of the two techniques, keeping the qualitative performance analysis of human interaction with the environment a study for future research.

## 6.2 Methodology

This section describes in detail the experimental setup for our study along with a brief discussion on data acquisition, preprocessing, feature extraction, and lastly the classification of different sets of data for their corresponding performance analysis.

### 6.2.1 Experimental Setup

Eleven healthy right handed-subjects (5 females and 6 males, mean age: 25.2 years old, range: 23-30 years old) participated in this study given their written informed consents. The study was performed at the Artificial Intelligence

Laboratory of Jadavpur University, Kolkata. All of these subjects were casual drivers while none of them had prior training on the experimental procedure in the present study.

EEG experiments were performed in a well insulated room. Subjects were seated comfortably in a chair similar to a car-driver seat. The EEG signals were recorded from a 32-channel Nihon Kohden EEG device using 21 electrodes. EEG signals were acquired using 19 electrodes from different brain regions [6]: prefrontal lobe electrodes (Fp1 and Fp2 ), frontal lobe electrodes (Fz, F3, F4, F7, and F8), occipital lobe electrodes (O1 and O2), parietal lobe electrodes (Pz, P3, and P4), motor cortex electrodes (Cz, C3, and C4) and temporal lobe electrodes (T3, T4, T5 and T6). The data sampling rate was set at 500Hz. The driving simulations were carried out using a standard LOGITECH driving simulator comprising a steering wheel, pedal foot, break foot, and a gear-box. Project CARS 2 ®© motorsport racing simulator having VR support along with HTC Vibe pro head-mount VR system were used for crating a VR-driving environment.

### 6.2.2 Data Acquisition

Each session required a participant to perform the driving task using the setup mentioned in the previous subsection, for a duration of 15 minutes and every participant completed the session twice (first without VR, and then with VR), not necessarily one after the other. The EEG device collected the brain samples corresponding to the 19 electrodes placed on the scalp in synchronous with the driving simulation. The recorded data for each session was then stored in a MATLAB (.m) file for further processing.

### 6.2.3 Preprocessing and Feature Extraction

As our objective was to analyze the cognitive load for driving corresponding to 7 different actions - acceleration (Acc), steering right (R), steering left (L), applying breaks (B), accident (Accd), chase (Ch), and slow-driving (Sl), the data samples corresponding to only these instances were extracted from the data acquired for each session, and each of them were stored as independent files. The acquired EEG signals were then passed through e-LORETA software [19] to detect the active brain regions responsible for the present learning task. The EEG signals acquired from the selected active brain lobes were then fed to the artifact removal unit to remove spurious noise effects. In this regard, Independent Component Analysis (ICA) [14] is performed over the EEG signals to extract scalp maps for each electrode position. An Elliptical Infinite Impulse response (IIR) filter was also used to filter the desired frequency band of the EEG responsible for motor learning. In the present context, we used two bio-physiological signals: P300 and N400, also known as event-related potentials (ERPs) for detection of visual alertness and proper learning over the entire learning phase. Then we use Principal Component Analysis (PCA) [15] to select the optimal features from a large dimension of extracted ERP features. Lastly, three statistical features, viz., mean( $\mu$ ) variance( $\sigma^2$ ) and kurtosis( $k$ ), of the respective data corresponding to each of these different scenarios were calculated.

### 6.3 Classifier Design

In the present learning problem, we propose a fuzzy classifier using GT2FS [16] to classify the data points. A GT2FS is a three tuple  $\langle x, u_{\bar{A}}(x), \mu(x, u_{\bar{A}}(x)) \rangle$ , where  $x$  is a linguistic variable (here, feature value),  $u_{\bar{A}}(x)$  is the primary member function (MF) and  $\mu(x, u_{\bar{A}}(x))$  is the secondary MF. Both the primary and the secondary MFs lie in  $[0,1]$ . Now, let  $x_i$  be an extracted EEG feature having  $r$  experimental instances,  $x_i^1, x_i^2, \dots, x_i^r$ , taken on the same day on the same subject. Presuming that the instances of  $x_i$  support Gaussian distribution, we represent them by a Gaussian MF with mean  $x_i$  and variance  $\sigma_i^2$  equal to the mean and variance of  $x_i^1, x_i^2, \dots, x_i^r$ . This Gaussian Type-1 MF represents that the instances of  $x_i$  are close enough to the mean value of the points. So, this MF is referred to as  $\mu_{close-to-mean}(x_i)$  abbreviated as  $\mu_C(x_i)$ .

We take the minimum and maximum of different type-1 MFs over different trials  $k$  to define a type-2 fuzzy set (T2FS), which is more complete than its type-1 counterpart. The T2FS thus obtained is represented by two type-1 MFs, called Upper MF (UMF) and Lower MF (LMF), given by

$$\bar{\mu}_{\bar{C}}(x_i) = UMF(x_i) = \max_{\forall j \in [1,k]} (\mu_C^j(x_j)). \quad (2.1)$$

$$\underline{\mu}_{\bar{C}}(x_i) = LMF(x_i) = \min_{\forall j \in [1,k]} (\mu_C^j(x_j)). \quad (2.2)$$

Thus for  $m$  features, we have  $m$  T2FS given by  $[\bar{\mu}_{\bar{C}}(x_i), \underline{\mu}_{\bar{C}}(x_i)]$ . Thus the foot of uncertainty (FOU) is obtained. The constructed FOU is then approximated by joining the peaks of Type-1 MFs with a straight line of zero slope to obtain a flat top UMF to confirm convexity and normality [20] of the type-2 fuzzy set, as described in Fig. 2.

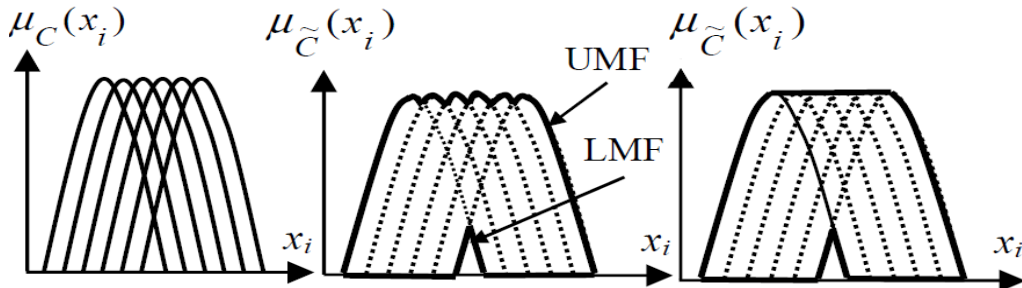


Figure 6.1: Construction of Flat-top IT2FS: (a) type-1 MFs, (b) IT2FS representation of (a), (c) flat-top approximated IT2FS

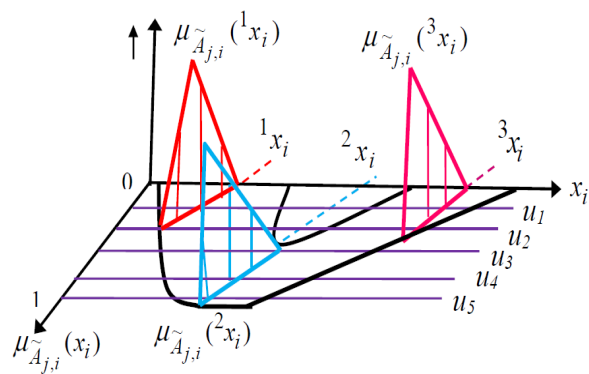


Figure 6.2: Secondary Membership Assignment

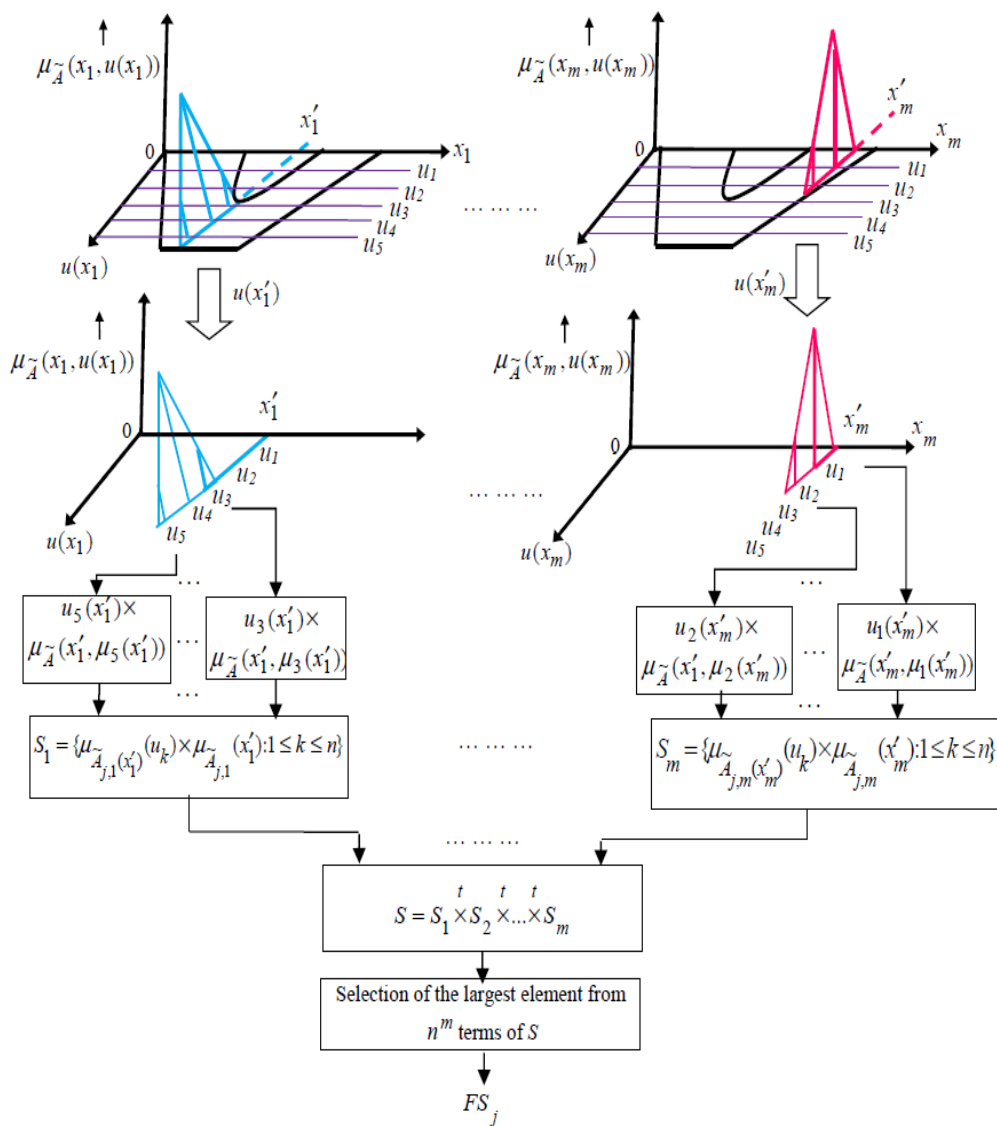


Figure 6.3: Firing Strength computation in the proposed GT2FS induced classification



## Type-2 Fuzzy Inference Generation

Let us consider, the classifier rule  $j$ , given by

*If  $x_1$  is  $\tilde{A}_{1,j}$  and  $x_2$  is  $\tilde{A}_{2,j}$  and ... and  $x_n$  is  $\tilde{A}_{n,j}$ , then class is  $j$*

where  $x_i$ ,  $i = 1$  to  $m$  are GT2FS-induced propositions. Here, we represent a GT2FS in vertical slice form (Fig. 3) [14], [21] where each vertical slice stands for secondary MF with respect to primary membership at a given  $x = x'$  say.

Suppose we have the measurements:  $x_i = x'_i$  for  $i = 1$  to  $m$  Let

$$S_i = \mu_{\tilde{A}_{j,i}(x'_i)}(u_k) \times \mu_{\tilde{A}_{j,i}(x'_i)}(x'_i) : 1 \leq j \leq k \quad (2.3)$$

and again let

$$S_p^T \times S_q = (\mu_{\tilde{A}_{j,p}(x'_p)}(u_b) \times \mu_{\tilde{A}_{j,p}(x'_p)}(x'_p))^T (\mu_{\tilde{A}_{j,q}(x'_q)}(u_g) \times \mu_{\tilde{A}_{j,q}(x'_q)}(x'_q)) \quad (2.4)$$

Then we obtain the firing strength of rule  $j$  in three steps (Fig. 4). 1. Evaluate,  $S = \Pi S_i \forall i$  terms in  $S$ .

2. Obtain the largest of the  $k^m$  terms in  $S$  and call it  $FS_j$
3. If  $FS_j > FS_l, \forall l \in [l, c]$ , where  $c$  is the number of classes

## 6.4 Experiments Results and Discussion

This section first details on the experimental results obtained through both the simulation techniques and then performs a comparative analysis to evaluate the performance variation of the two.

Table 6.1: Classification Accuracy without and with VR

Driving Action	Non-VR (%)	VR (%)
Acceleration	79.3	84.4
Break	83.9	87.5
Slow Driving	71.5	79.5
Right	76.5	82.8
Left	75.2	82.2
Chase	80.8	83.7
Accident	85.1	92.6
Average	78.9	86.1

#### 6.4.1 Comparative Analysis

Using the classifier designed in the previous section we evaluate the performance analysis if the two in terms of their classification accuracy, as shown in Table 2.1, and it could be observed that the classification accuracy of driving instances using VR is far superior than that without VR.

#### 6.4.2 Statistical Validation

Table 2.2 presents the results of the statistical test obtained by applying well-known Mc Nemar's test [16]. Here, we consider two classifier algorithms  $X$  and  $Y$ , where  $X$  is the proposed IT2FS classifier algorithm and  $Y$  is one of the other standard classifiers listed in Table 2.2. Let us define two parameters  $n_{01}$  and  $n_{10}$  where  $n_{01}$  be the number of classes misclassified by  $X$  but not by  $Y$  On the other hand,  $n_{10}$  be the number of classes misclassified by  $Y$  but

Table 6.2: Statistical analysis with the reference algorithm: proposed IT2Fs classifier

Classifier algorithm used for comparison using desired features	Parameters used for McNemar's test		z	Comments on acceptance/rejection of hypothesis
	$n_{01}$	$n_{10}$		
LSVM	31	97	33.01	Rejected
Type-1 Fuzzy	23	49	8.68	Rejected

not by  $X$ . Then, we define,

$$z = \frac{(|n_{01} + n_{10}| - 1)^2}{n_{01} + n_{10}}. \quad (2.5)$$

According to the  $\chi^2$  distribution table, we have  $\chi_{1,0.95}^2 = 3.38$  represents the value of Chi-square with probability 0.05 and the degree of freedom 1. The null hypothesis, representing that the two classifiers have identical performance with respect to the given classifier accuracy, is rejected as  $z$  exceeds  $\chi_{1,0.95}^2 = 3.84$

## 6.5 Conclusion

Through this work we can conclude that VR-based driving obviously has a better simulation performance that that compared to without VR case. Also, with the classification results obtained, we can get an insight that since the cognitive load while driving in a VR scenario is more compared to that of without VR, the classifier response is reflected correspondingly. Also, this work can stand as a strong motivation to all the future driving

---

simulation research to be based on our-proposed cost-efficient VR setup for better evaluation of their simulation results.

## References

- [1] A. Saha, A. Konar, R. Burman, and A.K. Nagar, "EEG analysis for cognitive failure detection in driving using neuro-evolutionary synergism", 2014 International Joint Conference on Neural Networks (IJCNN), pp. 2108-2115. IEEE, 2014.
- [2] A. Saha, S. Basu Roy, A. Konar, and R. Janarthanan, "An EEG-based cognitive failure detection in driving using two-stage motor intension classifier", In Proceedings of The 2014 International Conference on Control, Instrumentation, Energy and Communication (CIEC), pp. 227-231. IEEE, 2014.
- [3] A. Saha, A. Konar, M. Dan, and S. Ghosh, "Decoding of motor imagery potentials in driving using DE-induced fuzzy-neural classifier", 2015 IEEE 2nd International Conference on Recent Trends in Information Systems (ReTIS), pp. 416-421. IEEE, 2015.
- [4] A. Saha, A. Konar and A. K. Nagar, "EEG Analysis for Cognitive Failure Detection in Driving Using Type-2 Fuzzy Classifiers," in IEEE Transactions on Emerging Topics in Computational Intelligence, vol. 1, no. 6, pp. 437-453, Dec. 2017.

- 
- [5] L. Ghosh, A. Konar, P. Rakshit, S. Parui, A. L. Ralescu and A. K. Nagar, "P-300 and N-400 Induced Decoding of Learning-Skill of Driving Learners Using Type-2 Fuzzy Sets," 2018 IEEE International Conference on Fuzzy Systems (FUZZ-IEEE), Rio de Janeiro, pp. 1-8, 2018
- [6] L. Ghosh, A. Konar, P. Rakshit and A. K. Nagar, "Hemodynamic Analysis for Cognitive Load Assessment and Classification in Motor Learning Tasks Using Type-2 Fuzzy Sets," in IEEE Transactions on Emerging Topics in Computational Intelligence, vol. 3, no. 3, pp. 245-260, June 2019.
- [7] A. Van Dam, et al., "Experiments in immersive virtual reality for scientific visualization", Computers & Graphics, 26, no. 4, pp. 535-555, 2002
- [8] J.R. Wilson and Mirabelle D'Cruz, "Virtual and interactive environments for work of the future", International Journal of Human-Computer Studies 64, no. 3, pp. 158-169, 2006.
- [9] I. Karaseitanidis, et al., "Evaluation of virtual reality products and applications from individual, organizational and societal perspectives—The "VIEW" case study", International Journal of Human-Computer Studies 64, no. 3, pp. 251-266, 2006.
- [10] U. Anirudh, et al., "Assessing the Driver's Current Level of Working Memory Load with High Density Functional Near-infrared Spectroscopy: A Realistic Driving Simulator Study", Frontiers in Human Neuroscience, vol. 11, 2017.

- 
- [11] W. Konstantin, et al., "Multitasking During Simulated Car Driving: A Comparison of Young and Older Persons", *Frontiers in Psychology*, vol. 9, 2018.
- [12] Sportillo, Daniele, Alexis Paljic, and Luciano Ojeda. "Get ready for automated driving using Virtual Reality." *Accident Analysis & Prevention* 118, pp. 102-113, 2018
- [13] R. Sébastien, et al., "Can a Subjective Questionnaire Be Used as Brain-Computer Interface Performance Predictor?", *Frontiers in Human Neuroscience*, vol. 12, 2019.
- [14] A. Hyvärinen, J. Karhunen, and E. Oja, "Independent component analysis", *John Wiley & Sons*, vol. 46, 2004.
- [15] H. Abdi, and L. J. Williams, "Principal component analysis", *Wiley interdisciplinary reviews: computational statistics* 2, pp. 433-459, 2010.
- [16] X. Sun and Z. Yang, "Generalized McNemar's test for homogeneity of the marginal distributions", *SAS Global Forum*, 382, pp. 1-10, March, 2008.

# 7

## Conclusion

The thesis makes us a attempt for application in fuzzy logic. There are four applications of fuzzy logic in real world systems which have proposed. Firstly we have discussed about fuzzy and Brain computer Interface The first application deals with control of pH by neuro fuzzy decision making. The second application is concerned with EEG-based classification of fingers from finger tapping experiments. The third application refers to the analysis of functional near Infrared Spectroscopic images to classify individual finger movements. The last topic includes an analysis of cognitive load of the subject in a virtual-reality environment. Each topic is discussed with sufficient details, narrating the problem-description, approach, analysis, experiments and main results obtained at the end of the experiment.